Bao, Jichen; Somvanshi, Tejas; Tian, Yufang; Laird, Maxime G.; Garcia, Pierre Simon; Schöne, Christian; Rother, Michael; Borrel, Guillaume; Scheller, Silvan

Nature AND nurture: enabling formate-dependent growth in Methanosarcina acetivorans

Published in:
FEBS Journal

DOI:
10.1111/febs.17409

Published: 01/05/2025

Document Version
Publisher's PDF, also known as Version of record

The FEBS Journal

FEBS PRESS science publishing by scientists

Nature AND nurture: enabling formate-dependent growth in *Methanosarcina acetivorans*

Jichen Bao[1], Tejas Somvanshi[1], Yufang Tian[1], Maxime G. Laird[1], Pierre Simon Garcia[2], Christian Schöne[3], Michael Rother[3], Guillaume Borrel[2] and Silvan Scheller[1]

1 Department of Bioproducts and Biosystems, School of Chemical Engineering, Aalto University, Espoo, Finland
2 Evolutionary Biology of the Microbial Cell, Institut Pasteur, Université Paris Cité, UMR CNRS6047, France
3 Institute of Microbiology, Technische Universität Dresden, Germany

Keywords
ferredoxin; formate dehydrogenase; metabolic engineering; methane; *Methanosarcina*

Correspondence
J. Bao and S. Scheller, Department of Bioproducts and Biosystems, School of Chemical Engineering, Aalto University, Espoo FI-02150, Finland
Tel: +358 50 356 5175 (SS)
E-mail: baojichen@hotmail.com (JB); silvan.scheller@aalto.fi (SS)

Jichen Bao and Tejas Somvanshi contributed equally to this work.

(Received 9 August 2024, revised 8 November 2024, accepted 10 January 2025)

doi:10.1111/febs.17409

Methanosarcinales are versatile methanogens, capable of regulating most types of methanogenic pathways. Despite the versatile metabolic flexibility of Methanosarcinales, no member of this order has been shown to use formate for methanogenesis. In the present study, we identified a cytosolic formate dehydrogenase (FdhAB) present in several Methanosarcinales, likely acquired by independent horizontal gene transfers after an early evolutionary loss, encouraging re-evaluation of our understanding of formate utilization in Methanosarcinales. To explore whether formate-dependent (methyl-reducing or CO_2-reducing) methanogenesis can occur in Methanosarcinales, we engineered two different strains of *Methanosarcina acetivorans* by functionally expressing FdhAB from *Methanosarcina barkeri* in *M. acetivorans*. In the first strain, *fdhAB* was integrated into the N^5-methyl- tetrahydrosarcinapterin:coenzyme M methyltransferase (*mtr*) operon, making it capable of growing by reducing methanol with electrons from formate. In the second strain, *fdhAB* was integrated into the F_{420}-reducing hydrogenase (*frh*) operon, instead of the *mtr* operon, enabling its growth with formate as the only source of carbon and energy after adaptive laboratory evolution. In this strain, one CO_2 is reduced to one methane with electrons from oxidizing four formate to four CO_2, a metabolism reported only in methanogens without cytochromes. Although methanogens without cytochromes typically utilize flavin-based electron bifurcation to generate the ferredoxins needed for CO_2 activation, we hypothesize that, in our engineered strains, reduced ferredoxins are obtained via the *Rhodobacter* nitrogen fixation complex complex running in reverse. Our work demonstrates formate-dependent methyl-reducing and CO_2-reducing methanogenesis in *M. acetivorans* that is enabled by the flexible nature of the microbe working in tandem with the nurturing provided.

Abbreviations
ALE, adaptive laboratory evolution; BV, benzylviologen; CODH/ACS, carbon monoxide dehydrogenase/acetyl-CoA synthase complex; CoM, coenzyme M; cWLP, carbonyl branch of the Wood–Ljungdahl pathway; DPI, diphenyleneiodonium chloride; Ech, energy-converting hydrogenase; FBEB, flavin-based electron bifurcation; Fd, ferredoxin; Fdh, cytosolic formate dehydrogenase; Fdn, membrane-bound formate dehydrogenase; Fpo, $F_{420}H_2$ dehydrogenase; H_4MPT, tetrahydromethanopterin; H_4SPT, tetrahydrosarcinapterin; HdrABC, heterodisulfide reductase; HDS, CoM-S-S-CoB heterodisulfide; KP, potassium phosphate buffer; Mcr, methyl-coenzyme M reductase; MP, methanophenazine; Mtr, methyl-H_4SPT:HS-CoM methyltransferase; MvhAGD, methyl viologen-reducing hydrogenase; mWLP, methyl branch of the Wood–Ljungdahl pathway; OD_{600}, attenuance at 600 nm; Rnf, *Rhodobacter* nitrogen fixation complex; Vht, methanophenazine-reducing hydrogenase.

Introduction

Methanogens are anaerobic archaea that produce methane via their energy metabolism [1,2]. The most widespread methanogenesis pathway uses H_2 as the electron donor to reduce CO_2 to methane (hydrogenotrophic CO_2-reducing methanogenesis) (Fig. 1A) [3]. The reduction of CO_2 to methane involves the methyl branch of the Wood–Ljungdahl pathway (mWLP), the methyl-tetrahydrosarcinapterin (H_4SPT):coenzyme M (CoM) methyltransferase (Mtr) membrane-bound complex and the methyl-coenzyme M reductase (Mcr) [4–6]. In the mWLP, CO_2 is sequentially reduced to a methyl group starting on methanofuran and transferred to either tetrahydromethanopterin (H_4MPT) or H_4SPT (H_4MPT analogue in *Methanosarcina*). At the end of the mWLP pathway, membrane-bound Mtr transfers the methyl group from H_4MPT or H_4SPT to the cofactor CoM. The energy released by this methyl transfer is used to translocate Na^+ across the membrane, forming a chemiosmotic gradient that can be exploited by an ATP synthase. Mcr then reduces the methyl group bound to CoM to methane by oxidizing the thiol CoB-SH to form the CoM-S-S-CoB heterodisulfide (HDS). Most hydrogenotrophic methanogens do not rely on electron transport through the membrane that involves cytochromes and membrane-soluble electron carriers. They are termed 'methanogens without cytochromes' and include methanogens that belong to the orders Methanobacteriales, Methanopyrales, Methanococcales, Methanocellales, Methanomassiliicoccales and Methanomicrobiales [1,7]. The cytosolic electron carriers ferredoxin (Fd), F_{420} and CoB-SH are used to transfer electrons from H_2 to the C1-unit being reduced to methane. $F_{420}H_2$ is used for the two reduction steps occuring at H_4MPT, where the C1-unit undergoes a four-electron reduction from the oxidation state of a formyl group to a methyl group [5]. The reduction of F_{420} to $F_{420}H_2$ can be carried out by the F_{420}-reducing hydrogenase (i.e. FrhABG) with electrons coming directly from H_2 [5,8]. The first step, reduction of CO_2, is catalyzed by either tungsten-dependent or molybdenum-dependent formylmethanofuran dehydrogenase (i.e. Fwd or Fmd) [4]. The reduction is particularly challenging and therefore requires the strongly reducing Fd_{red} [9–11]. The low-potential Fd_{red} cannot be directly obtained from electrons from H_2. In methanogens without cytochromes, they are generated via flavin-based electron bifurcation (FBEB) by the cytoplasmic heterodisulfide reductase (HdrABC)–[NiFe]–methyl viologen-reducing hydrogenase (MvhAGD) enzyme complex [1,12,13]. Here, two molecules of H_2 are oxidized and, at the same time, Fd_{ox} is reduced to Fd_{red} and HDS is reduced to CoM-SH and CoB-SH. Many CO_2-reducing methanogens without cytochromes can also use formate as an alternative electron donor to H_2 (Fig. 1A) [5]. In this case, the reduction of F_{420} involves an FdhAB complex. FdhA is a formate dehydrogenase and FdhB is an F_{420}-oxidoreducase homologous to FrhB [14]. In addition, FdhAB replaces the MvhAG hydrogenase to form a FdhAB–MvhD–HdrABC complex for the reduction of Fd_{ox} and HDS via FBEB [15]. Fd_{red} is not only required for catabolic CO_2 reduction in the first step of methanogenesis, but also for anabolic purposes [16,17]. Anabolism starts with the formation of the C2 compound, acetyl-CoA. This compound is synthesized from a methyl group generated by the mWLP and is combined with the carbonyl group from the carbonyl branch of the

Fig. 1. Hydrogenotrophic methanogensis in methanogens without cytochromes (A), the three major methanogenesis pathways in *M. acetivorans* (B–D) and the electron transport system in *Methanosarcina* (E, F). (A) Hydrogenotrophic methanogenesis in methanogens without cytochromes utilize H_2 or formate to reduce CO_2. The Fd_{red} for methanogenesis is regenerated by FBEB, whereas the Fd_{red} for anabolism is regenerated by Eha/Ehb [18,19]. (B) Acetoclastic methanogenesis: the carbonyl carbon of acetate is oxidized to obtain Fd_{red}. This Fd_{red} is then used to reduce HDS, which is the terminal electron acceptor in methanogenesis. (C) Methylotrophic methanogenesis: 1 molecule of methanol is oxidized to CO_2 to provide 2 $F_{420}H_2$ and 1 Fd_{red} that are then used to reduce 3 molecules of HDS formed from 3 molecules of methanol reduced to methane. (D) CO-dependent CO_2-reducing methanogenesis, Fd_{red} are obtained from oxidizing CO to CO_2. *M. acetivorans* uses an uncharacterized system to cycle electrons from Fd_{red} to $F_{420}H_2$ [83]. (E) H_2-independent electron transport system of *M. acetivorans*. (F) H_2-dependent electron transport system of *M. barkeri*, which is capable of all four (A–D) methanogenesis pathways but uses H_2 as a sole electron source or as an intermediate. All reduced cofactors are in orange and the oxidized counterparts are in blue. Chemical equations and ATP yield per methane produced from respective pathways at the bottom. For simplicity, some reactants (e.g. free HS-CoM) are not shown. Enzymes: carbon monoxide dehydrogenase/acetyl-CoA synthase complex (CODH/ACS), methyl-H_4SPT:HS-CoM methyltransferase (Mtr), $F_{420}H_2$ dehydrogenase (Fpo), heterodisulfide reductase (Hdr), *Rhodobacter* nitrogen fixation complex (Rnf), formate dehydrogenase (Fdh), F_{420}-reducing hydrogenase (Frh), [NiFe]-hydrogenase (Mvh), methanophenazine-reducing hydrogenase (Vht), energy-converting hydrogenases (Eha/Ehb/Ech), methanol methyltransferase (Mta) and methyl-CoM reductase (Mcr). FBEB, flavin-based electron bifurcation; HDS, CoM-S-S-CoB heterodisulfide; Fd_{red}, reduced ferredoxin. Created with Biorender.com.

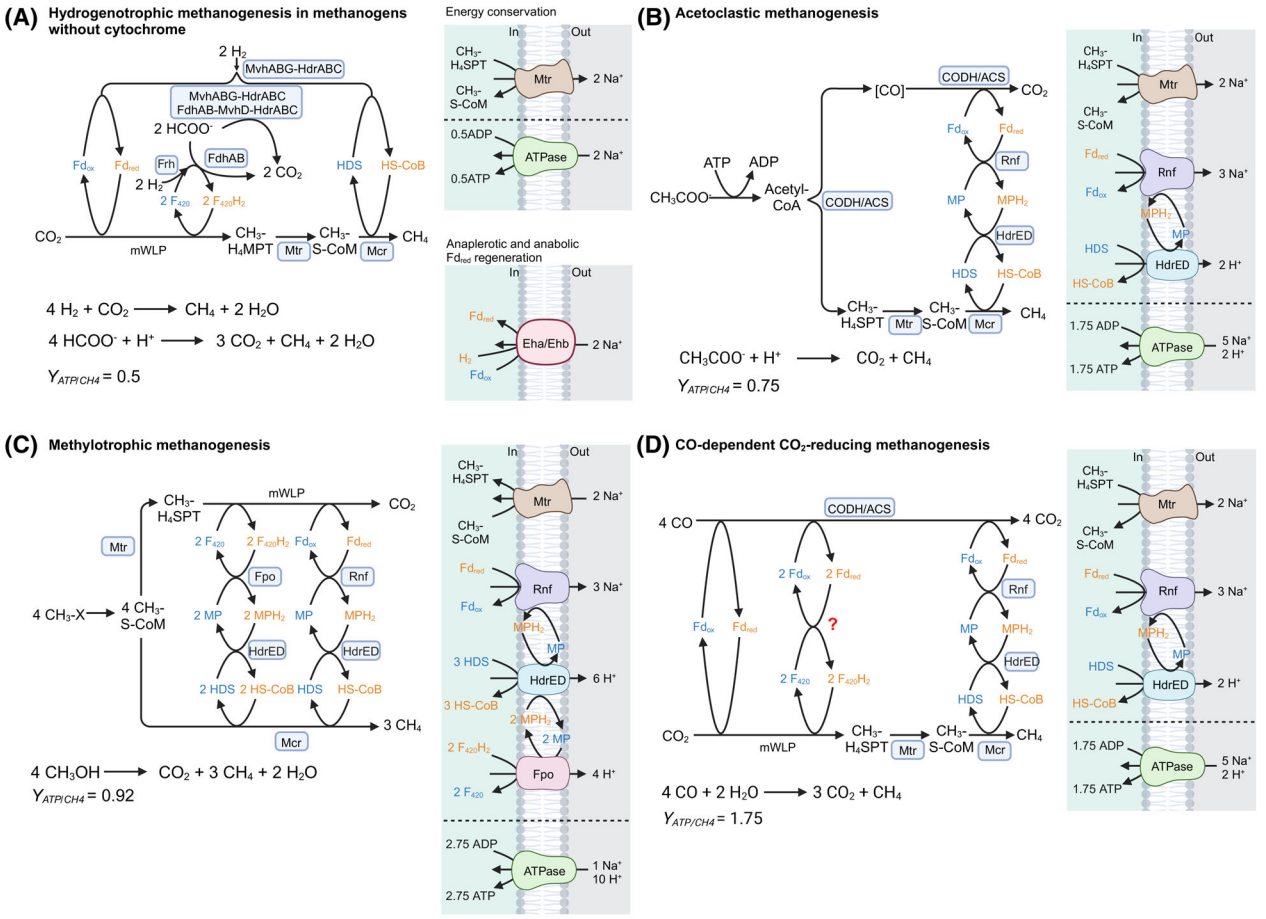

WLP (cWLP) that relies on the carbon monoxide dehydrogenase/acetyl-CoA synthase (CODH/ACS) complex. Next, an additional Fd_{red} is needed to convert acetyl-CoA and CO_2 to the C3 compound, pyruvate. Pyruvate is then carboxylated to the C4 compound, oxaloacetate, which is the starting point for gluconeogenesis and for amino acid biosynthesis via the incomplete citric acid cycle [17]. The Fd_{red} needed for CO_2 fixation in anabolism can be generated by a range of membrane-bound energy-converting hydrogenases, such as the Eha or Ehb complex in Methanococcales [18,19]. These membrane-bound hydrogenases couple the endergonic reduction of the Fd_{ox} by H_2 with consumption of the transmembrane chemiosmotic gradient.

Methanosarcinales, which are the focus of the present study, rely on cytochromes for their energy metabolism [1,7]. Distinctive features in their methanogenesis pathways include the unique ability to disproportionate methyl-compounds (methylotrophic methanogenesis) or acetate (acetoclastic methanogenesis). Although most methanogens can only use one

type of carbon compound (CO_2 or methyl-compound) as electron acceptor, many *Methanosarcina* species can shift between several methanogenesis pathways. Depending on the substrate, the mWLP, CODH/ACS and Mtr are combined in different ways, and their direction may be reversed. The diversity of methanogenesis pathways in *Methanosarcina* and their energy metabolism is briefly summarized in Fig. 1 [7,20–22]. In acetoclastic methanogenesis, the carbonyl group of acetate is oxidized into CO_2 by CODH/ACS, providing electrons for the reduction of the methyl group of acetate into methane (Fig. 1B). In methylotrophic methanogenesis, one methyl group from the substrate is oxidized into CO_2 through the mWLP, providing electrons to reduce three methyl groups into methane (Fig. 1C). For the oxidation of the methyl-group to CO_2, Mtr uses the chemiosmotic gradient to perform the endergonic transfer of the methyl group from CoM to H_4SPT and the mWLP functions in the oxidative direction. The CO-dependent CO_2-reducing pathway operates in similar principle of disproportionation. The electrons obtained from oxidation of CO to CO_2 by CODH/ACS are used to reduce CO_2 to methane via mWLP (Fig. 1D). In all methanogenesis pathways of *Methanosarcina*, the chemiosmotic gradient is built via membrane-bound electron transport from either H_2, $F_{420}H_2$ or Fd_{red} to HDS (Fig. 1E,F) [7,23]. Irrespective of the source of electrons, the membrane-soluble electron transporter methanophenazine (MP) is reduced by membrane-bound complexes. MPH_2 is re-oxidized via the HdrED complex that transfers electron from MPH_2 to HDS. *Methanosarcina* species have an $F_{420}H_2$:HDS electron transport pathway that is H_2-independent, where the F_{420} dehydrogenase (Fpo) oxidizes $F_{420}H_2$ to reduce MP. *Methanosarcina* species that can utilize H_2, such as *M. barkeri*, have an H_2-dependent electron transport system (Fig. 1F), where H_2 can be the sole source of electrons in the H_2:HDS electron transport pathway that involves the methanophenazine-reducing hydrogenase (Vht). H_2 can also be an intermediate in the $F_{420}H_2$:HDS and the Fd_{red}:HDS electron transport pathway involving the Frh or the energy-converting hydrogenase (Ech), respectively. The electron transport system of *M. acetivorans*, however, is H_2-independent (Fig. 1E). Here the Fd_{red}:HDS electron transport pathway involves the *Rhodobacter* nitrogen fixation complex (Rnf) that oxidizes Fd_{red} to reduce MP [7]. FBEB from Fd_{red} to HDS and F_{420} has also been suggested to occur through the cytosolic HdrABC complex in *M. acetivorans*, which is present in two copies in its genome. The HdrA1B1C1 complex has been shown to play a role in methylotrophic methanogenesis [24]. The HdrA2 subunit from *M. acetivorans* contains a fused mvhD domain and the HdrA2B2C2 has been shown to play a role in acetoclastic methanogenesis [24,25]. An absence of *ech* and no expression of *vht* prevents *M. acetivorans* from hydrogenotrophic CO_2-reducing methanogenesis and formation of Fd_{red} from either internal cycling of H_2 or external H_2 [26–28]. A putative alternative option to generate Fd_{red} could be the HdrABC or the Rnf complex running in reverse, which has been currently shown only *in vitro* [25,29,30].

Despite the metabolically versatile nature of *Methanosarcina*, formate utilization as an electron donor for CO_2 or methyl reduction has never been reported in such species. However, formate dehydrogenase activity has been previously reported in *M. barkeri* grown on methanol, as well as the presence of *fdhAB* in the genome of this methanogen and *Methanosarcina mazei* [31–33]. Along with FdhAB, the presence of the formate transporter has been suggested to be required for growth on formate [34]. However, at high concentrations of formate and low pH, formate could passively diffuse into the cells in the form of formic acid [35]. There are no formate transporters annotated in the genome of *M. barkeri* or *M. mazei* but genes encoding AceTr family proteins are present in the genome and have been shown capable of formate transport in *Saccharomyces cerevisiae* [36,37]. The lack of formate-dependent CO_2 reduction in *Methanosarcina* that contain an H_2-dependent electron transport system has been hypothesized to be a result of the high H_2 threshold that would be required by the Ech complex to generate Fd_{red} [1,38]. Formate utilization by methanogens with cytochrome has only been reported in members of the Methanonatronarchaeales for methyl reduction. These methanogens employ a membrane-bound formate dehydrogenase (Fdn), in which FdnG is homologous to FdhA, to directly transfer electrons from formate to MP [39]. Whether Methanosarcinales members could utilize formate as electron donor for CO_2 or methyl reduction by this way or using a different pathway is unknown. *M. acetivorans* provides a unique opportunity to test this because its genome encodes the genes for AceTr family proteins, and it has an H_2-independent electron transport system that relies on the Rnf complex along with cytosolic HdrABC complexes.

In the present study, we explored the capacity of Methanosarcinales to use formate as a source of carbon and energy. First, we evaluated the phyletic distribution and evolution of the formate dehydrogenase in this order, revealing a surprisingly large number of

copies in acetoclastic *Methanotrichaceae* and a patchy distribution in *Methanosarcinaceae*, acquired by horizontal gene transfer. Unlike *Methanonatronarchaeia*, all formate dehydrogenases are predicted to be cytosolic. Then, we show that one of these Methanosarcinales, *M. barkeri*, can consume formate when growing on methanol and we validated the activity of its formate dehydrogenase by expressing it in *M. acetivorans*. We further investigated how the formate dehydrogenase of *M. barkeri* can be accommodated in the metabolic pathways of *M. acetivorans* by engineering two different strains. The first strain *M. acetivorans* JB-MF (*mtr::fdhAB*) became capable of growing by reducing methanol with electrons from formate. The second strain *M. acetivorans* JB-F2 (*frh::fdhAB*) became capable of growing on formate as the only source of carbon and energy, a metabolism that was previously reported only for methanogens without cytochromes. Finally, we constructed strains *M. acetivorans* JB-MF Δ*hdrA1*, *M. acetivorans* JB-MF Δ*hdrA2* and *M. acetivorans* JB-MF $rnfB^{E63X}$ to obtain insights on how Fd_{red} is regenerated during formate-dependent CO_2-reducing and methyl-reducing methanogenesis.

Results

Distribution and phylogeny of the F_{420}-reducing formate dehydrogenase

Homologs of FdhA were searched in a database comprising 9596 bacterial and 1268 archaeal proteomes, including 68 Methanosarcinales. FdhA is prevalent among methanogens belonging to the lineages most closely related to the Methanosarcinales, namely Methanocellales, Methanoflorentales (Bog-38), Methanomicrobiales and Halobacteriales (Fig. 2A). By contrast, Methanosarcinales exhibit an uneven distribution of FdhA, with a comparatively lower number of genomes encoding it. On one hand, all *Methanotrichaceae* (a basal lineage in Methanosarcinales) genomes contain at least one *fdhA* gene and most of them have between three and seven copies of this gene. On the other hand, FdhA is only present in eight out of the 43 *Methanosarcinaceae* in our database (Fig. 2A). The phylogeny of FdhA revealed that this gene was acquired multiple times through horizontal gene transfer during the evolution of Methanosarcinales (Fig. 2B). These horizontal gene transfer events in *Methanosarcinaceae* are further supported by the patchy distribution of the enzyme in this family. Indeed, vertical inheritance in *Methanosarcinaceae* species is unlikely because it would imply many losses, including many recent losses in *Methanosarcina*. The phylogeny of FdhA also indicates that the multiple copies present in *Methanotrichaceae* originate from several horizontal gene transfers rather than gene duplication (Fig. 2B). All identified *fdhA* genes in Methanosarcinales form a genomic cluster with *fdhB*, indicating the presence of a cytosolic FdhAB formate dehydrogenase, rather than a membrane-bound, cytochrome-containing FdnGHI formate dehydrogenase, as in *Methanonatronarchaeia* [40,41].

Formate consumption by *M. barkeri* WWM155 and characterization of its FdhAB

We re-evaluated formate consumption in *M. barkeri* WWM155 (used as wild type in this study) by growing it on methanol and formate. Under this condition, *M. barkeri* did not produce higher methane levels than with methanol alone. Formate consumption and increased acetate production in presence of formate was confirmed through ^{1}H-NMR spectroscopic quantification (Table 1). Similar to previously published studies, our attempts to grow *M. barkeri* using formate as the sole source of carbon and energy failed [32]. To validate the activity of FdhAB and check for functional expression, it was heterologously produced in *M. acetivorans* WWM73, used as wild-type in the present study. *fdhAB* was expressed from a plasmid under the control of P*mcrB*(tetO1) promoter [42]. The activity of the recombinant enzyme was assessed by measuring its ability to reduce benzyl viologen in cell-free extracts, which yielded an activity of 0.7 $U \cdot mg^{-1}$ total protein (Fig. 3) that confirms functional expression in *M. acetivorans* WWM73.

Effect of formate on *M. acetivorans* WWM73

To gather physiological reference before incorporating formate dehydrogenase in *M. acetivorans*, we cultivated the parent strain WWM73 in HSMe (i.e. high salt medium with 60 mM methanol only) and MF (i.e. high salt medium with 60 mM methanol and formate each) media. The strain consumed all methanol in either medium and did not consume any formate in MF medium (Fig. 4C,D) but the maximum attenuance at 600 nm (OD_{600}) and methane yield was slightly lower in presence of formate (Fig. 4A,B). The strain grew slower in the presence of formate (doubling time of approximately 8 h) than in its absence (doubling time of approximately 7 h) (Fig. 4A) and produced more acetate when formate was present similar to *M. barkeri* (Fig. 4E). The pH of the medium did not change either with addition of formate at beginning of growth or at the end because formate was not

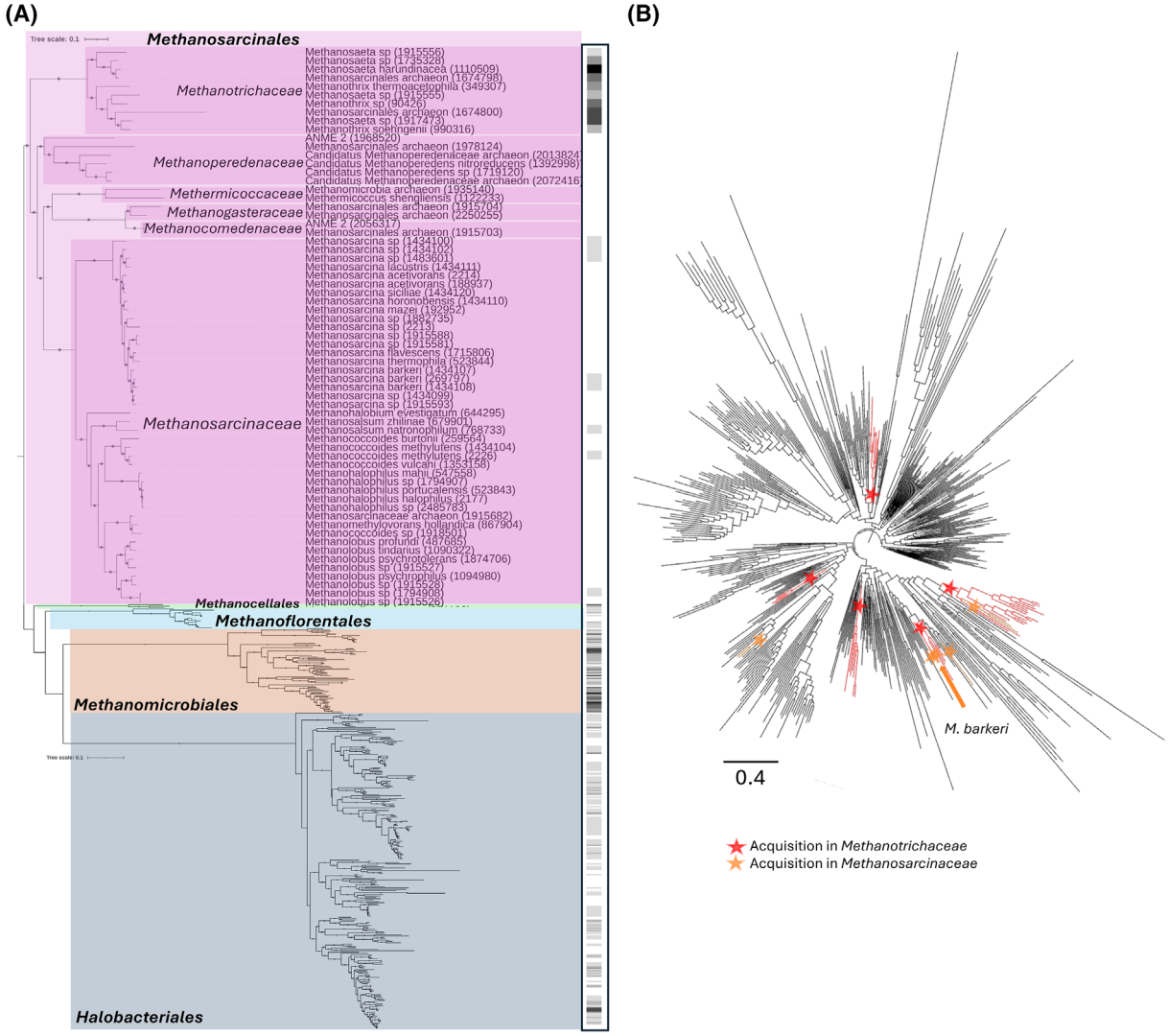

Fig. 2. Taxonomic distribution and phylogenetic tree FdhA. (A) Taxonomic distribution of FdhA in class II methanogens and *Halobacteriales*. The phylogenetic tree has been inferred based on a concatenation of If2, RpoB and RpoC alignments (LG + F + R10 + C20 + PMSF, 383 sequences, 2523 amino-acid positions) using FASTTREE v2.1.10. The dots at the nodes correspond to ultrafast-bootstrap values > 95%. A zoom on the tree has been applied for Methanosarcinales. The number of copies of FdhA is represented by a gray gradient (white = 0, black = 7). The numbers in parenthesis at the tips correspond to the NCBI taxonomic ID. Scale bars represent the average number of substitutions per site. (B) Phylogenetic tree of FdhA (LG + R10, 540 sequences, 658 amino-acid positions) inferred using IQ-TREE v1.6.12. Stars represent independent acquisitions in Methanosarcinales. A subsampling of sequences has been applied for non-Methanosarcinales sequences. The scale bars represent the average number of substitutions per site. Generated using ITOL.

consumed. Transcriptomic data were acquired from three biological replicates to explore effects of formate on energy conservation pathway and identify possible candidates for formate transporters (AceTr family proteins). In presence of formate, 29 genes were significantly differentially expressed ($P_{adj} < 0.01$, $|\log_2 FC| \geq 2$) as described in Dataset S1; however, none of the 29 genes belonged to the energy conservation pathway or were AceTr family proteins. Although the transcriptomic analysis did not provide conclusive insight into the energy conservation pathway or formate transporter, the dataset may be a valuable resource for future studies and, as such, the raw reads have been uploaded to Sequence Read Archive database (https://www.ncbi.nlm.nih.gov/) and the raw dataset of differentially expressed genes is made available as Dataset S1.

With physiological reference obtained, the formate dehydrogenase of *M. barkeri* was accommodated in the metabolic pathways of *M. acetivorans* WWM73 by

Table 1. Formate consumption in *M. barkeri* WWM155. Media composition: MF, methanol (60 mM) + formate (60 mM); HSMe, methanol (60 mM). Data from three biological replicates. Values expressed as the mean ± SD. ****$P < 0.0001$ indicates a significant change between the media. Statistical significance was determined by two-tailed, two sample *t*-test.

	Metabolites measured at end of growth (312 h)			
Media	Methanol (mM)	Formate (mM)	Methane (μmol)	Acetate (mM)
MF methanol (60 mM) + formate (60 mM)	0	38.3 ± 1.2	260 ± 16	1.66 ± 0.01****
HSMe methanol (60 mM)	0	0.07 ± 0.01	240 ± 1.5	2.08 ± 0.02****

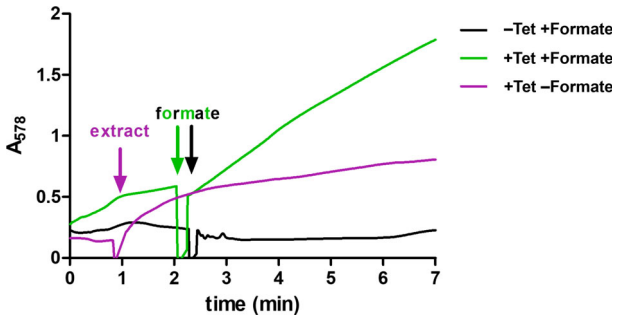

Fig. 3. *In vitro* activity of FdhAB from *M. barkeri* heterologously expressed in *M. acetivorans*. Cleared cell-free lysates were tested for reduction of benzylviologen (BV). Before preparation of cell-free lysates, the identical strain was cultured under different conditions ($n = 1$). Green line (experiment): expression of FdhAB was induced with tetracycline (Tet). The activity measured was 0.7 U·mg^{-1} total protein. Black line (control): FdhAB expression was not induced. Green and black arrows indicate addition of formate which colored green and black to match where it is added to the respective reaction mix. Purple line (control): expression of FdhAB was induced with Tet, but no formate was added to the assay. The increase in absorbance of the purple line is a result of non-specific reduction by FdhAB. For details, see Materials and methods.

engineering two different strains with two different metabolisms: *M. acetivorans* JB-MF capable of formate-dependent methyl-reducing methanogenesis (Fig. 5A) and *M. acetivorans* JB-F2 capable of formate-dependent CO_2-reducing methanogenesis (Fig. 5B).

Formate-dependent methyl-reducing methanogenesis

M. acetivorans JB-MF was constructed by inserting *fdhAB* from *M. barkeri* between the promoter and coding sequence of *mtr* operon of *M. acetivorans* WWM73, disrupting the *mtr* gene. *fdhAB* utilized the native promoter of *mtr* for transcription. We inserted one additional terminator at the end of *fdhAB* operon (*fpo* terminator from *M. barkeri* WWM155) to ensure that *mtr* is not expressed. Without the expression of *mtr*, the strain lost its ability to grow solely on methanol because our attempts to grow the strain in HSMe medium failed, similar to other previously published Δ*mtr* mutant strains of *M. acetivorans* [43,44]. The exogenous FdhAB, however, enabled formate-dependent methyl-reducing methanogenesis in *M. acetivorans* JB-MF (Fig. 5A).

The doubling time of *M. acetivorans* in MFAcP medium (60 mM methanol and formate, each; 5 mM acetate and pyruvate, each) was approximately 11 h (Fig. 6A). Acetate and pyruvate were added to the medium as anabolic substrates, because, in the absence of Mtr, methanol cannot be oxidized to CO_2 to generate the Fd_{red} required for anabolism [44]. Apart from anabolism, oxidation of acetate could also provide the electrons for reducing methanol. Metabolite analysis showed that all formate, methanol, and acetate was consumed by the end of growth, and that the methane yield reached the maximal theoretical value (Fig. 6B–E). The strain was also able to grow in absence of acetate and pyruvate (MF medium). The doubling time was approximately 15 h (Fig. 6A). Metabolite analysis showed that all formate was consumed by the end of growth, but 15.7 ± 0.8 mM methanol remained (Fig. 6C,D). The pH of the MFAcP and MF media did not change at the end of growth. Throughout the growth, the ratio of formate oxidized per methanol reduced reached a maximum of

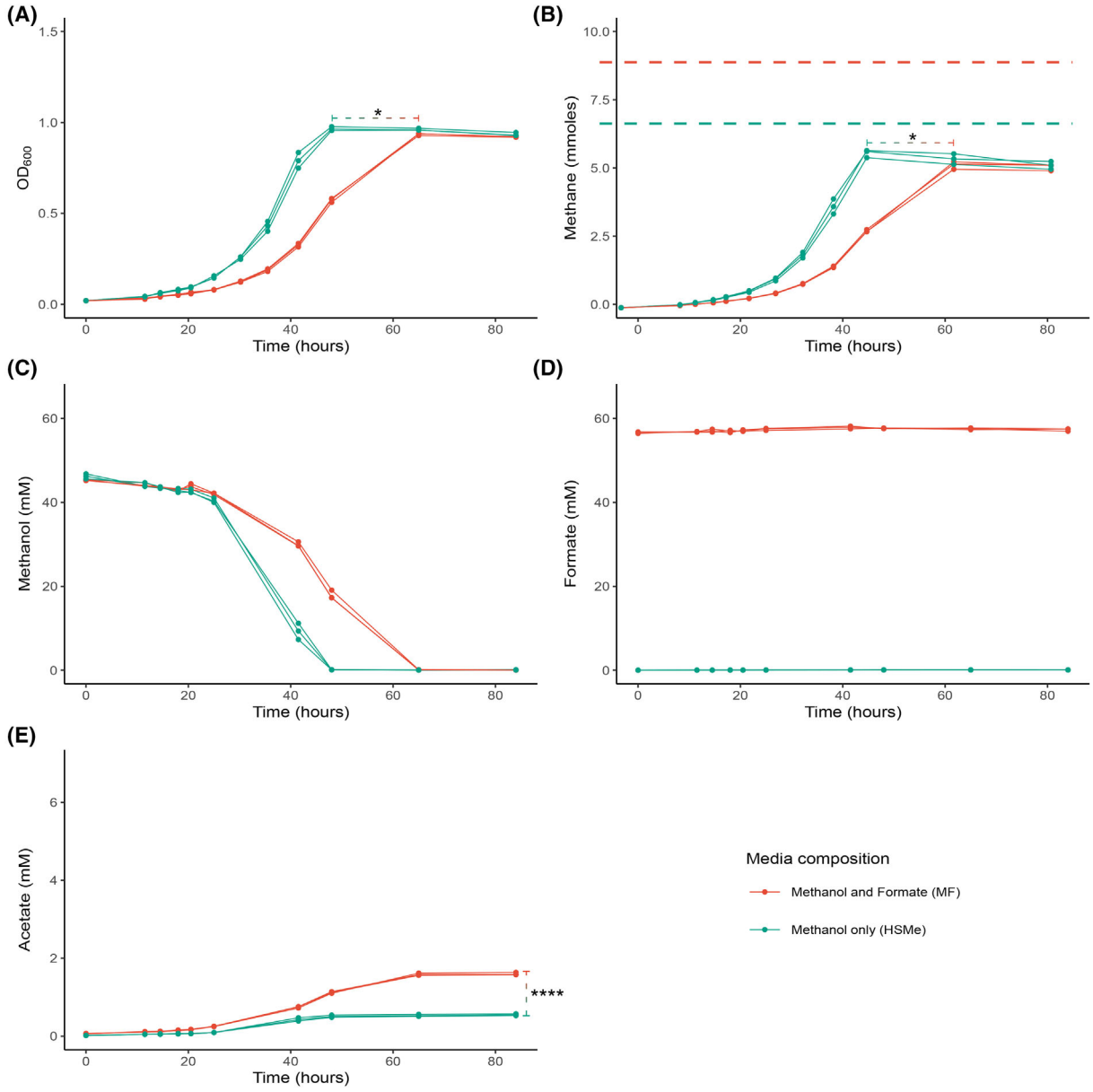

Fig. 4. Influence of formate on growth of *M. acetivorans* WWM73. The strain was grown in HSMe (60 mM methanol) (green) and MF (60 mM methanol + 60 mM formate) (red) media. (A) OD_{600}: doubling time in HSMe medium (approximately 7 h) was significantly lower ($P < 0.0001$) than in MF medium (approximately 8 h). (B) Methane level (mmol). Dashed lines represent theoretical yield of methane for methanol disproportionation (green) and for a hypothetical scenario where all methanol could be reduced to methane using electrons from formate (red). (C) Methanol level (mM). (D) Formate level (mM). (E) Acetate level (mM). Growth curve and metabolite curves obtained from three independent cultures (all shown). Statistical significance was determined by two-tailed two sample *t*-test for OD_{600}, methane, acetate and growth rates, as well as by a one-tailed two sample *t*-test for formate. ****$P < 0.0001$ and *$P < 0.05$ indicate a significant change between the media. OD_{600} and methane were compared at maximum values but different timepoints. Formate consumption was non-significant ($P > 0.05$) compared between $T = 0$ and $T = 84$ h.

1.7 : 1, which deviated from the expected 1 : 1 ratio. Growth of the strain without added acetate and pyruvate indicates that the strain can produce Fd_{red} required for anabolism and CO_2 fixation from electrons obtained by oxidation of formate.

Transcriptomic data were acquired to gain possible insights into the Fd_{red} regeneration and anabolic pathways in *M. acetivorans* JB-MF when growing without added acetate and pyruvate. In absence of acetate and pyruvate, 58 genes were significantly differentially

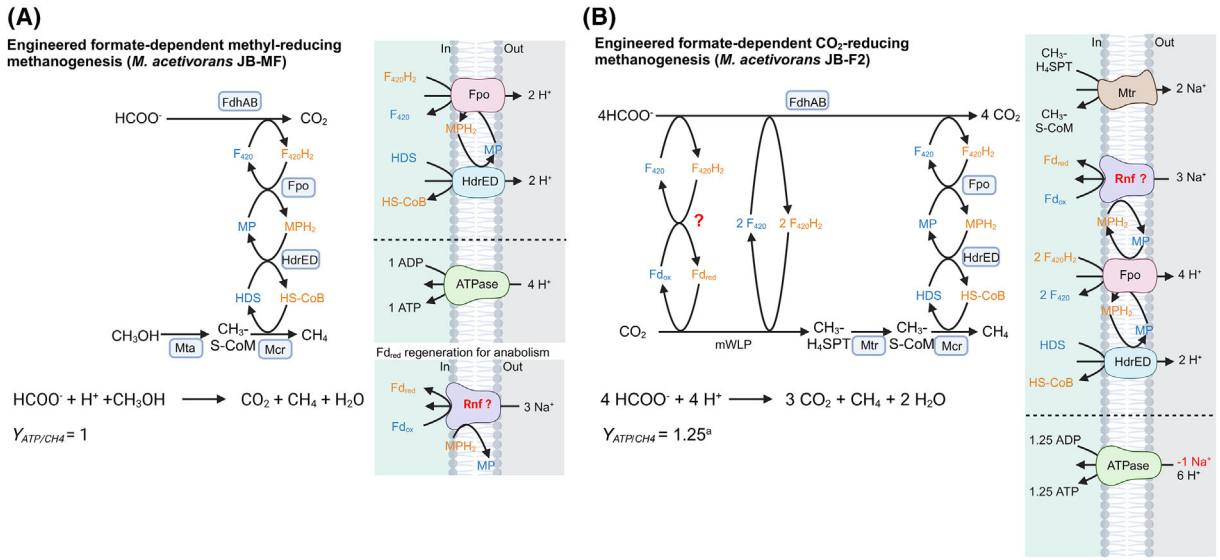

Fig. 5. The engineered formate-dependent methyl-reducing methanogenesis pathway in *M. acetivorans* JB-MF and formate-dependent CO2-reducing methanogenesis pathway in *M. acetivorans* JB-F2. (A) Engineered formate-dependent methyl-reducing methanogenesis (strain JB-MF)–formate is oxidized to reduce the HDS formed from methyl-CoM reduction. Fd_{red} for anabolism is made available putatively via Rnf. (B) Engineered formate-dependent CO_2-reducing methanogenesis (strain JB-F2)–formate disproportionation leads to formation of 3 CO_2 and 1 CH_4. The yet-unknown step (marked in red question mark) is how Fd_{red} is obtained from formate oxidation for CO_2 reduction. Putatively, the most important contributor is Rnf. All reduced cofactors are in orange and the oxidized counterparts are shown in blue. Chemical equations and ATP yield per methane produced from respective pathways are at the bottom. [a]ATP yield as calculated from the hypothetical Rnf-based energy pathway and thermodynamic estimations (for details, see Materials and methods and Fig. 8). For simplicity, some reactants (e.g. free HS-CoM) are not shown. Enzymes: methyl-H_4SPT:HS-CoM methyltransferase (Mtr), $F_{420}H_2$ dehydrogenase (Fpo), heterodisulfide reductase (Hdr), *Rhodobacter* nitrogen fixation complex (Rnf), formate dehydrogenase (Fdh), methanol methyltransferase (Mta) and methyl-CoM reductase (Mcr). HDS, CoM-S-S-CoB heterodisulfide; Fd_{red}, reduced ferredoxin. Created with Biorender.com.

expressed ($P_{adj} < 0.01$, $|\log_2 FC| \geq 2$) as described in Dataset S2. We expected to see *rnf* or *hdrABC* genes to be upregulated in absence of acetate and pyruvate to enable the microbe to regenerate Fd_{red}; however, *rnf* and *hdrABC* genes were not significantly upregulated, which, although not confirming their involvement, does not imply the lack of it in Fd_{red} regeneration. Although the transcriptomic analysis did not support or refute this hypothesis for Fd_{red} regeneration, we found the genes *fwd*, *mcr* and *mta* upregulated in the absence of acetate and pyruvate. *ma4393*, a gene encoding AceTr family protein, was also upregulated in MF medium compared to MFAcP medium. The dataset may be a valuable resource for future studies and, as such, the raw reads have been uploaded to Sequence Read Archive database and the raw dataset of differentially expressed genes is made available as Dataset S2.

Testing redundancy in the energy and ferredoxin metabolism via deletions in JB-MF

The following three different enzyme complexes were hypothesized to contribute to the generation of Fd_{red} when operating in the reverse direction: HdrA1B1C1, HdrA2B2C2 and Rnf [24,25,29,30,45]. To test their putative involvement, an attempt was made to delete each of these enzyme complexes in the strain JB-MF because transcriptomic comparisons did not provide concrete evidence. HdrA is the flavin containing subunit of the HdrABC complex that is the site for FBEB. *M. acetivorans* JB-MF Δ*hdrA1* and *M. acetivorans* JB-MF Δ*hdrA2* were constructed and tested for their ability to grow on MF medium where additional carbon sources such as acetate and pyruvate were absent (Table 2). Δ*hdrA2* could grow in MF medium; however, Δ*hdrA1* mutant had a prolonged lag phase of 12–14 days in MF medium. Neither deletion abolished growth in MF medium.

Multiple attempts to delete the entire *rnf* operon via CRISPR-Cas and replacement by *pac* cassette failed. Finally, we were able to disrupt the *rnf* operon by a nonsense mutation in the *rnfB* gene, which encodes the subunit that is the 'wire conduit' of electrons enabling interaction of Fd_{red} and the Rnf complex [46]. The *M. acetivorans* JB-MF $rnfB^{E63X}$ mutant had lost the ability to grow in MF medium (Table 2). The essentiality of Rnf for growth in MF medium hints towards its important role in Fd_{red} regeneration, using the chemiosmotic gradient to reduce Fd_{ox} with MPH_2 as electron donor.

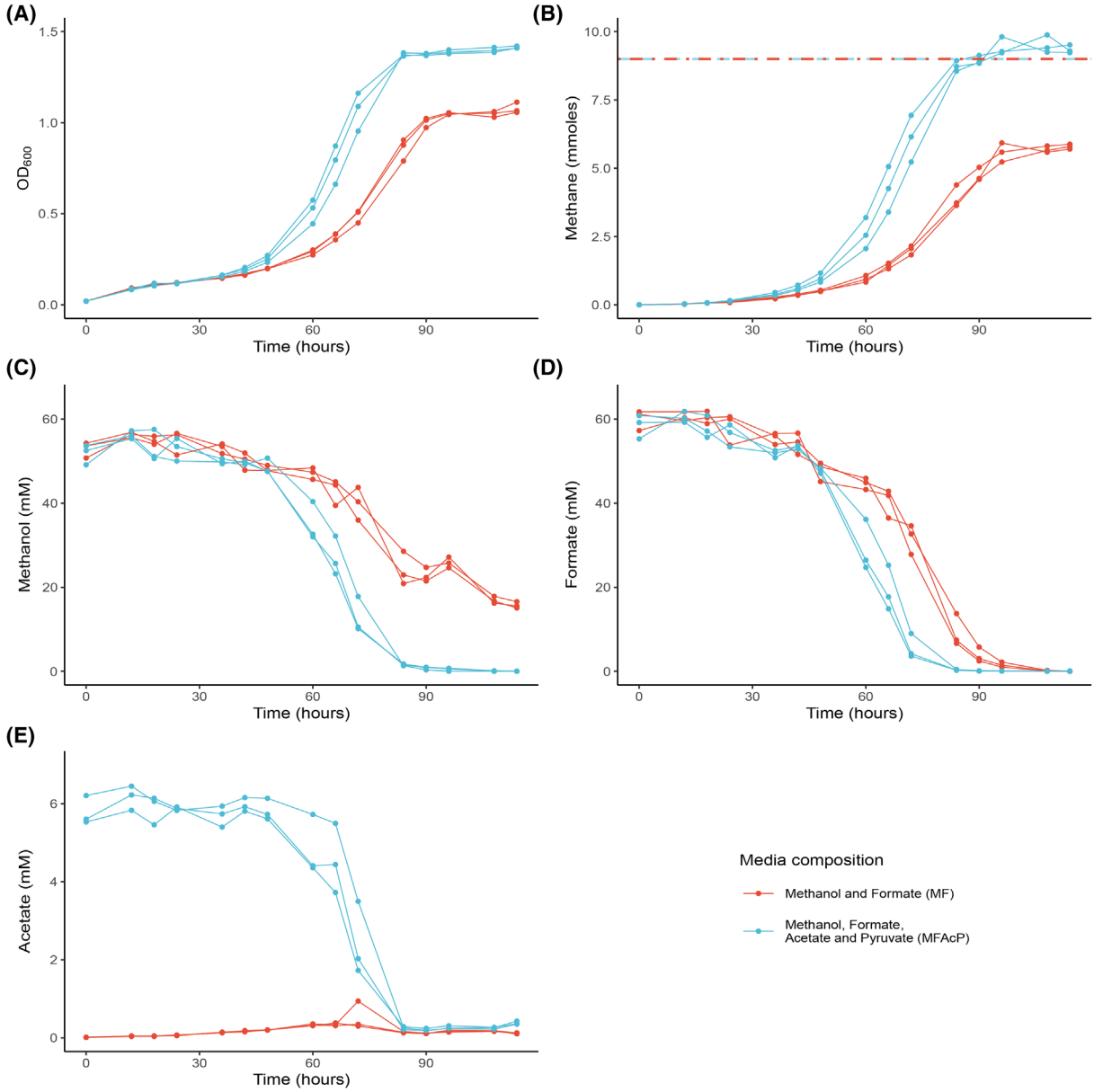

Fig. 6. Growth of *M. acetivorans* JB-MF with formate-dependent methyl-reducing methanogenesis. The strain was grown in MF (red) (60 mM methanol + 60 mM formate) and MFAcP (blue) (60 mM methanol + 60 mM formate + 5 mM acetate + 5 mM pyruvate) media. (A) OD_{600}: doubling time in MF medium (approximately 15 h) and MFAcP medium (approximately 11 h). (B) Methane level (mmol). Dashed red and blue line represents theoretical yield of methane in MF and MFAcP media. Methane level in MFAcP medium reaches theoretical yield as all methanol is reduced. The difference between measured methane level and theoretical methane yield is not statistically significant [$P > 0.05$, two-tailed one sample *t*-test for (B)]. (C) Methanol level (mM). 15.7 ± 0.8 mM methanol remained in MF medium at the end of growth. (D) Formate level (mM). (E) Acetate level (mM). Growth curve and metabolite curves obtained from three independent cultures (all shown).

Formate-dependent CO_2-reducing methanogenesis

To determine whether *M. acetivorans* could be able to use formate as a sole source of carbon and energy, we engineered a second *M. acetivorans* strain by integrating *fdhAB* into the *frh* operon under the control of *mtr* promoter from *M. acetivorans* C2A (Fig. 5B). The strain obtained, *M. acetivorans* JB-F1, was able to grow solely on formate because *mtr* was not disrupted, but the doubling time of

Table 2. Energy metabolism redundancy. Media composition: MF, methanol (60 mM) + formate (60 mM). Data from three biological replicates.

Strain/genotype	Growth in MF media
M. acetivorans JB-MF Δ*hdrA2*	Yes
M. acetivorans JB-MF Δ*hdrA1*	Yes, long lag phase (12–14 days)
M. acetivorans JB-MF *rnfB*^{E63X}	No growth observed after 10 weeks of cultivation

methanogenesis was approximately 80 h. *M. acetivorans* JB-F1 was subjected to adaptive laboratory evolution (ALE) to increase fitness and to be able to grow faster solely on formate in HSF medium (High salt medium with 120 mM formate only). The serial transfers of *M. acetivorans* JB-F1 were started from methanol medium into rich formate medium containing casamino acids along with 5 mM acetate and 5 mM pyruvate and was later transferred to HSF medium (Fig. 7F). At the end of 32 repeated serial transfers (see Materials and methods), ALE shortened doubling time of methanogenesis of strain JB-F2 (designation given at the end of ALE) from approximately 80 h to 11 h when growing solely on formate (Fig. 7B,F). The difference of doubling time of *M. acetivorans* JB-F2 in HSMe (approximately 12 h) and HSF (approximately 13 h) media was not statistically significant ($P > 0.05$, two-tailed two sample *t*-test); however, JB-F2 took longer to reach maximum OD_{600} (Fig. 7A) in HSF medium. The biomass yield of JB-F2 growing on formate was 2.48 g total protein mol^{-1} CH_4, which was higher than the other growth conditions investigated in this study (Table 3). When *M. acetivorans* JB-F2 grew solely on formate, approximately 11 mM formate (8% of initially added formate) remained at the end of growth with the rest going towards methane, biomass and acetate (Fig. 7D), whereas all methanol was consumed when *M. acetivorans* JB-F2 was grown solely on methanol (Fig. 7C). The pH of the HSF medium increased to 7.8 when monitored at the end of growth. *M. acetivorans* JB-F2 produced over 3 mM acetate when growing solely on formate (Fig. 7E).

The genomes of selected stages during ALE were sequenced and analyzed. All single nucleotide polymorphisms are listed in Table S1. Only one structural variation, a 332-bp deletion in *fwdD1*, was observed in the genome. *fwdD1* encodes the subunit D of tungsten-dependent formylmethanofuran dehydrogenase [47]. To check whether deletion in *fwdD1* played a role in JB-F2, we recreated the deletion in *M. acetivorans* JB-F1 (strain before ALE), but this deletion failed to change the doubling time of methanogenesis in *M. acetivorans* JB-F1 Δ*fwdD1* when tested.

To test whether the electron transport was cytosolic or through membrane during formate-dependent CO_2-reducing methanogenesis, diphenyleneiodonium chloride (DPI) which is an MP analogue, was added to the growth media of *M. acetivorans* WWM73, JB-F2 and *Methanococcus maripaludis* J901 [48]. DPI has been shown to block electron transport in the membrane of *M. mazei*. DPI inhibited the growth of *M. acetivorans* JB-F2 and WWM73 but did not inhibit the growth of *M. maripaludis* J901, indicating that electron transport through membrane was still crucial for growth (Table 4).

Transcriptomic data were acquired for *M. acetivorans* JB-F2 growing on formate compared to growth on methanol to gain insights into possible genes involved in energy conservation during formate-dependent CO_2-reducing methanogenesis. *M. acetivorans* JB-F2 when grown on formate compared to methanol showed 23 significantly differentially expressed genes ($P_{adj} < 0.01$, $|\log_2 FC| \geq 2$) as described in Dataset S3. We expected to see changes in the transcription level of *rnf* and *hdrABC* genes to confirm that they are involved in the Fd_{red} regeneration pathway of *M. acetivorans* JB-F2. Although the transcriptomic analysis did not show any significantly different changes in the expression of *rnf* and *hdrABC*, it did show methanol-specific methyltransferases (*mtaCB1* and *mtaCB2*) highly downregulated ($\log_2 FC$ approximately −8 and −2.5, respectively) in JB-F2 when grown solely on formate. It is interesting to note that *ma4393* was significantly downregulated ($\log_2 FC$ of approximately −2.4) in JB-F2 when growing on formate. The dataset may be a valuable resource for future studies and, as such, the raw reads have been uploaded to Sequence Read Archive database and the raw dataset of differentially expressed genes is made available as Dataset S3.

Discussion

Distribution and evolution of FdhA in Methanosarcinales

The ubiquitous presence of *fdhA* and its multiple acquisitions in *Methanotrichaceae*, up to seven copies per genome, suggests that this enzyme has a key role in these methanogens. *Methanothrix soehngenii* cleaves formate into H_2 and CO_2 [49], demonstrating that *fdhA* is expressed, but none of the described *Methanothrix* species can use formate for methanogenesis [50,51]. A formate dehydrogenase activity has been previously reported in *M. barkeri* (19), as well as the presence of *fdhAB* in the

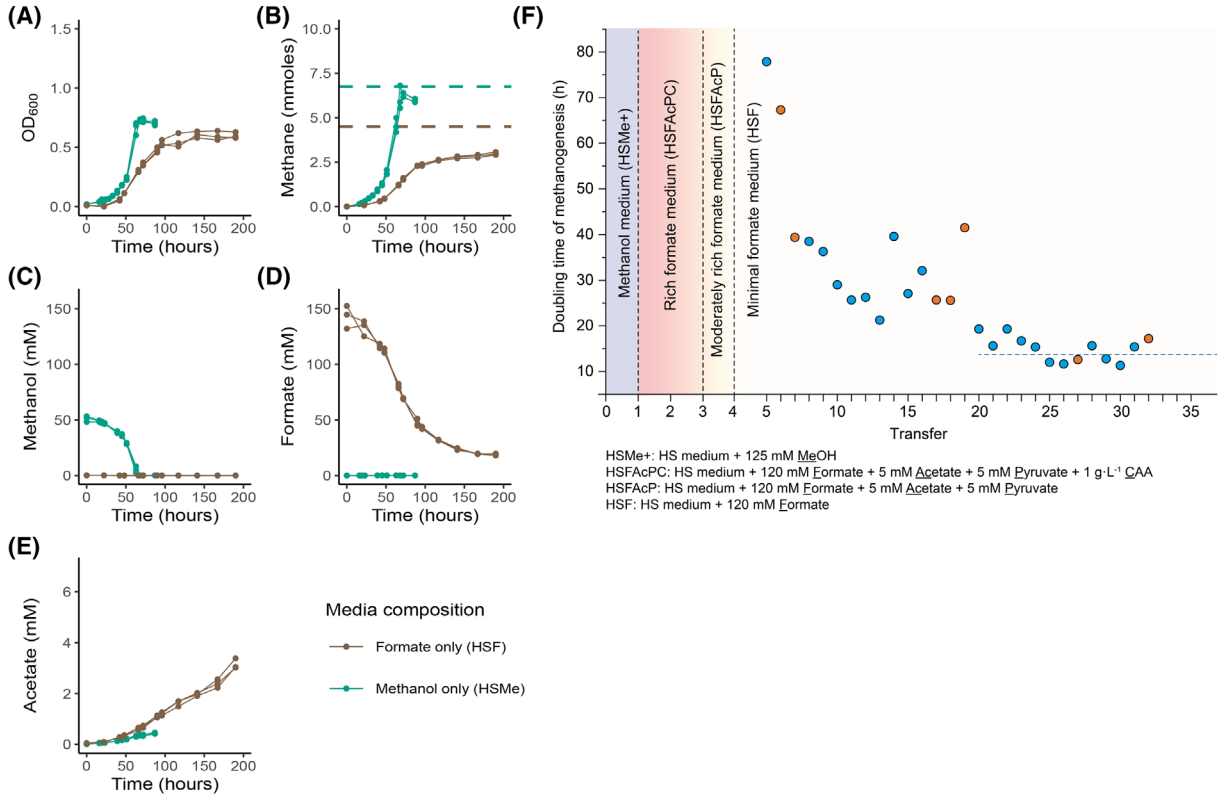

Fig. 7. Growth of *M. acetivorans* JB-F2 under two different conditions. Growth via well-established methylotrophic methanogensis (HSMe, green), and via the novel metabolism of formate-dependent CO_2-reducing methanogenesis (HSF, brown). All three replicates are shown (A) OD_{600}: doubling time in HSMe medium (approximately 12 h) was similar to HSF medium (approximately 13 h) ($P > 0.05$) (B) Methane level (mmol). Dashed lines represent theoretical yield of methane for each condition. (C) Methanol level (mM). (D) Formate level (mM). (E) Acetate level (mM). (F) Doubling time of methanogenesis during ALE. Vertical dashed lines indicate change in medium composition. Blue dashed horizontal line marks the average doubling time of methanogenesis for the transfer strains that the line spans. The ALE was performed as described in the Materials and methods to lower the doubling time of methanogenesis of strain JB-F1. The strain obtained from ALE was designated as JB-F2. Blue and orange dots track the doubling time of methanogenesis of which orange dots represent the transfer stages selected for genome sequencing. Statistical significance was determined by two-tailed two sample *t*-test for growth rates. ALE, adaptive lab evolution.

genome of *M. mazei*, but previous attempts to grow *M. barkeri* and other *Methanosarcinaceae* on formate alone failed [52]. The role of the formate dehydrogenase in these ecologically important methanogens needs to be clarified. Whether formate can be used as an electron donor for methanogenesis under yet undefined conditions, such as syntrophic partnership with bacteria, remains to be determined. For example, *Methanothrix* spp. are limited to acetate utilization in monoculture but can reduce CO_2 during growth in coculture, using direct electron transfer from syntrophic bacteria in this process [53]. It is possible that formate does play an anabolic role as seen in *M. barkeri*, where formate consumption did not lead to significant increase in methane production but instead led to increased acetate production (Table 1). This hints towards the possible anabolic role of formate in Methanosarcinales.

fdhA may have been present in the last common ancestor of the Methanosarcinales and was lost after the divergence between the *Methanotrichaceae* and other Methanosarcinales. Then, *fdhA* was re-acquired in some *Methanosarcinaceae*, including *M. barkeri*, through horizontal gene transfer. Multiple acquisition of this gene in *Methanosarcinaceae* and the present study presents a case for re-evaluation of the widespread belief of lack of formate metabolism in *Methanosarcinaceae*.

Natural capability of *M. acetivorans* towards formate utilization

Formate-dependent methyl-reducing and CO_2-reducing methanogenesis was made possible in *M. acetivorans* by heterologous expression of FdhAB (Fig. 5). However,

Table 3. Biomass yield of *M. acetivorans* on different growth media. Media composition: HSMe, methanol (60 mM); MF, methanol (60 mM) + formate (60 mM); MFAcP, methanol (60 mM) + formate (60 mM) + acetate (5 mM) + pyruvate (5 mM); HSF, formate (120 mM). Data from three biological replicates. Values expressed as the mean ± SD. The total protein was calculated by multiplying OD_{600} to the conversion coefficient 69.75 mg·L^{-1} $OD_{600}{}^{-1}$. The values were calculated based on the growth in the exponential phase. *$P < 0.05$, **$P < 0.01$ and ***$P < 0.0001$ indicates a significant change in JB-F2 grown in HSF medium compared to the respective condition. Statistical significance determined by one-way analysis of variance and the Bonferroni test.

Strain	Medium	$Y_{\text{total protein/CH4}}$ (g total protein mol^{-1} CH_4)
WWM73	HSMe	2.17 ± 0.02*
WWM73	MF	2.08 ± 0.03**
JB-MF	MFAcP	1.67 ± 0.04****
JB-MF	MF	2.01 ± 0.11****
JB-F2	HSMe	1.56 ± 0.10****
JB-F2	HSF	2.48 ± 0.13

Table 4. Growth of *M. acetivorans* WWM73, *M. acetivorans* JB-F2 and *M. maripaludis* J901 in media containing DPI. Media composition: HSMe, methanol (60 mM); MF, methanol (60 mM) + formate (60 mM); HSFAcP, formate (120 mM) + acetate (5 mM) + pyruvate (5 mM); HSF, formate (120 mM); McFC, formate (400 mM) with 5 g·L^{-1} casamino acids. Data from two biological replicates.

Strain	Media	DPI[a]	Growth
M. maripaludis J901	McFC	No	Yes
M. maripaludis J901	McFC	Yes	Yes
M. acetivorans WWM73	HSMe	No	Yes
M. acetivorans WWM73	HSMe	Yes	No
M. acetivorans JB-F2	HSMe	No	Yes
M. acetivorans JB-F2	HSMe	Yes	No
M. acetivorans JB-F2	HSF	No	Yes
M. acetivorans JB-F2	HSF	Yes	No
M. acetivorans JB-F2	HSFAcP	No	Yes
M. acetivorans JB-F2	HSFAcP	Yes	No

[a]DPI was dissolved in dimethyl sulfoxide. The same amount of dimethyl sulfoxide was added to the media that did not contain DPI.

this enzyme complex on its own may not be sufficient for formate utilization, indicating that *M. acetivorans* WWM73 already carries other genes allowing this activity. In *Escherichia coli*, *fdhD* has been shown to be essential for formate dehydrogenase activity [54]. FdhD, defined as 'formate dehydrogenase family accessory protein' catalyzes the sulfur transfer from *L*-cysteine desulfurase to formate dehydrogenase. The genome of *M. acetivorans* wild-type encodes a *fdhD* gene that could be as important as FdhAB for growth and methanogenesis from formate. The initial presence of this gene in absence of FdhAB, suggests that it may alternatively transfer sulfur to other target proteins.

There are no formate transporters annotated in the genome of *M. acetivorans* [55], suggesting that it either uses another transporter or relies on passive diffusion for formate intake. Given the importance of formate transporters seen in thermophilic methanogens, it is likely that *M. acetivorans* could use an uncharacterized formate transporter. Three genes encoding the AceTr family proteins, shown to support formate transport in *Saccharomyces cerevisiae* [37], are present in the genome of *M. acetivorans*. Out of the three, only one, *ma4008*, has been characterized and shown to be acetate specific [36]. Upregulation of *ma4393* in *M. acetivorans* JB-MF could have made it a promising candidate for formate transporter; however, downregulation of the same in *M. acetivorans* JB-F2 when growing on HSF medium questions the possibility. Additional characterization of proteins encoded by genes–*ma4393* and *ma0103*, would help determine whether either could support formate transport in *M. acetivorans*.

M. acetivorans WWM73 produced approximately 1.5 mM acetate in presence of formate but no formate was consumed. However, the maximum methane and OD_{600} measured was lower in presence of formate, suggesting that acetate is produced by rerouting the carbon from methanol to acetate instead of methane and biomass (Fig. 4). Acetate production was also seen in *M. acetivorans* JB-F2 where it produced approximately 3.6 mM acetate (Fig. 7E). The acetogenic potential of *M. acetivorans* has been discussed previously when growing on CO to make ATP from converting acetyl-phosphate to acetate [22].

Natural plasticity in the energy metabolism of *M. acetivorans* strain JB-MF

M. acetivorans JB-MF became capable of formate-dependent methyl-reducing methanogenesis with heterologous expression of formate dehydrogenase and disruption of *mtr*. When growing in MF medium, the expected ratio for formate oxidation to methanol reduction was 1 : 1, assuming only catabolism. Approximately 15 mM residual methanol, deviating from the 1 : 1 ratio, suggests that approximately 15 mM formate was consumed for anabolism to form approximately 3.75 mM acetyl-CoA (four formate to one acetyl-CoA) (Fig. 6C). The upregulation of *fwd* in MF medium could be in response to increased demand of CO_2 reduction for anabolism, whereas the

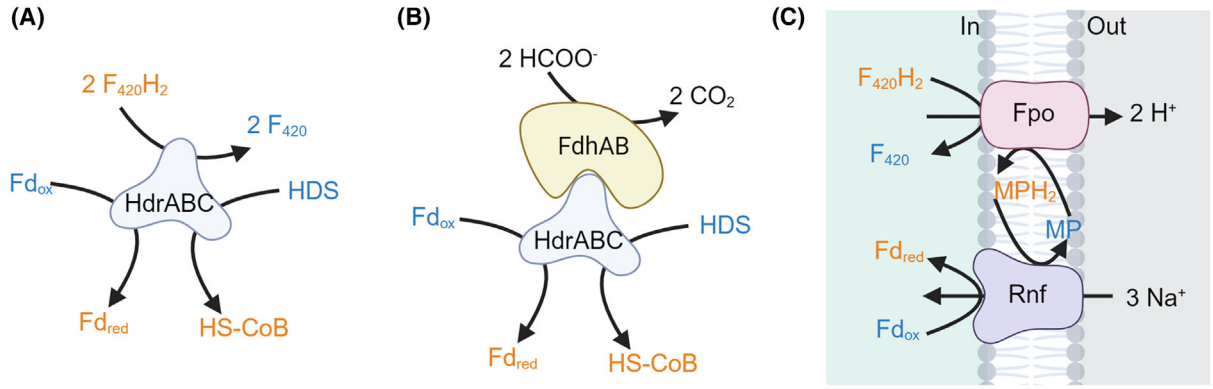

Fig. 8. The three possible pathways for generation of Fd_{red} (A–C). (A) FBEB by HdrABC in reverse by either HdrA1B1C1 or HdrA2B2C2. Two $F_{420}H_2$ are oxidized to reduce Fd_{ox} and HDS. (B) FBEB by FdhAB–HdrABC complex. We hypothesized that HdrA2 is involved in complex formation because it contains the MvhD domain fused to it. MvhD has been shown to be present in the FdhAB–MvhD–HdrABC complex from methanogens without cytochromes. (C) Fd_{ox} reduction by Rnf using electrons from MPH2 and chemiosmotic gradient. This reaction is the reverse of the proposed role of Rnf in *M. acetivorans*. All reduced cofactors are shown in orange and the oxidized counterparts are shown in blue. Enzymes: *Rhodobacter* nitrogen fixation complex (Rnf), $F_{420}H_2$ dehydrogenase (Fpo), heterodisulfide reductase (Hdr), formate dehydrogenase (Fdh). flavin-based electron bifurcation (FBEB), CoM-S-S-CoB heterodisulfide (HDS) and reduced ferredoxin (Fd_{red}). FBEB, flavin-based electron bifurcation; Fd_{red}, reduced ferredoxin; HDS, CoM-S-S-CoB heterodisulfide. Created with Biorender.com.

upregulation of *mta* and *mcr* could be in response to accumulated methanol and HDS as a result of the unavailability of additional formate as source of electrons. In MFAcP medium, an additional 5 mM each of acetate and pyruvate was provided. Oxidation of one acetate molecule completely through the mWLP and cWLP can provide electrons (2 $F_{420}H_2$ and 2 Fd_{red}) to reduce four methanol molecules to methane, implying approximately 3.75 mM acetate would be sufficient to reduce the remaining approximately 15 mM methanol. As seen at the end of growth in MFAcP medium, the additional acetate and pyruvate not only were consumed as anabolic substrates, but also provided electrons to reduce all the methanol provided. The plasticity in the energy metabolism of *M. acetivorans* to generate Fd_{red} may be enabled by the different possible options. The possible pathways are summarized in Fig. 8. Each of the three hypotheses are briefly discussed below: (a) the HdrABC enzyme [56–58], (b) the HdrA2B2C2 forming complex with FdhAB and [25] and (c) the membrane-bound Rnf running in reverse [29,30].

Electron bifurcation via the HdrABC enzyme

Both copies of HdrABC have been hypothesized to have the capability to bifurcate electrons from $F_{420}H_2$ to Fd_{ox} and HDS [24,25,58] (Fig. 8A). Out of the two copies in the genome of *M. acetivorans*, this capability has been verified biochemically only for HdrA2B2C2 [7,25]. The *M. acetivorans* JB-MF Δ*hdrA2* mutant, however, could grow in MF medium implying a lack of HdrA2B2C2 involvement in Fd_{red} regeneration. On the other hand, *M. acetivorans* JB-MF Δ*hdrA1* showed a prolonged lag phase in MF medium; however, Δ*hdrA1* did not abolish growth. The prolonged lag phase of Δ*hdrA1* has been reported previously in *M. acetivorans* for methylotrophic methanogenesis where it was hypothesized that HdrA1B1C1 is possibly used to bypass HdrED when the entire pool of MP is fully reduced [24]. Failure to abolish growth of Δ*hdrA2* and Δ*hdrA1* in MF medium discards FBEB solely via either copy of HdrABC as the possible pathway for Fd_{red} regeneration. The possibility of the other copy of HdrABC making up for the deletion of one, however, is not ruled out and could imply partial involvement of FBEB in Fd_{red} regeneration.

Electron bifurcation via the HdrA2B2C2 and FdhAB complex

The multienzyme complex responsible for FBEB from formate consists of HdrABC, FdhAB and MvhD [15,59,60] (Fig. 8B). There is no *mvhD* annotated gene in *M. acetivorans* but the HdrA2 of *M. acetivorans* has been shown to have a fused MvhD domain [7,25]. Similar to *Methanomicrobiales*, the HdrABC from *M. acetivorans* could form a complex with FdhAB to enable FBEB from formate to HDS and Fd_{ox}. However, as mentioned above, *M. acetivorans* JB-MF Δ*hdrA2* mutant could grow in MF medium, discrediting this

hypothesis, and showing a lack of involvement of Fdh–Hdr complex in Fd_{red} regeneration.

Membrane-bound Rnf running in reverse

The Rnf complex couples the oxidation of Fd_{red} to the reduction of MP and pumps out 3 Na^+ during this process in *M. acetivorans* [7,23,61] (Fig. 8C). In other microbes, Rnf has shown to demonstrate the activity of Fd:NADH oxidoreductase [30]. Using a Na^+ gradient, it was able to catalyze endergonic reduction of Fd_{ox} using NADH [30]. A similar reduction of Fd_{ox} could be possible in *M. acetivorans* where the chemiosmotic gradient is built through Fpo and MPH_2 replaces NADH as the source of electrons. The lack of growth of *M. acetivorans* JB-MF $rnfB^{E63X}$ mutant in MF medium supports the hypothesis of Rnf being essential in Fd_{red} regeneration.

Formate as the sole carbon and energy source in Methanosarcinales

M. acetivorans JB-F2 grows by a metabolic pathway novel to the Methanosarcinales order and to cytochrome-containing methanogens (Fig. 5B). Formate-dependent CO_2-reducing methanogenesis in *M. acetivorans* JB-F2 highlights the strains capability to produce Fd_{red} required for CO_2 reduction and anabolism without using H_2 as an intermediate, providing evidence for high H_2 thresholds as the limiting factor for formate utilization in Methanosarcina with H_2-dependent electron transport system [1]. Although FdhAB enabled CO_2 reduction to methane, the process was slow in the beginning, which was remedied by ALE, increasing the fitness of the strain on formate. Although JB-F2 exhibits a catabolism similar to methanogens without cytochromes, cytochromes are still required for the formate-dependent CO_2-reducing methanogenesis in *M. acetivorans* JB-F2 as confirmed by growth inhibition as a result of DPI.

The present study opens the way to better understand the mysterious formate metabolism in Methanosarcinales. Genomic integration of a functional *fdhAB*, along with ALE, enabled formate-dependent methanogenesis in *M. acetivorans*. This remarkable finding could only be possible by *M. acetivorans* meeting us halfway with its flexibility and redundancy in the energy metabolism. Formate dependent methanogenesis in *M. acetivorans* may be considered an example of 'nature' (i.e. the plasticity of metabolism towards formate and Fd_{red} regeneration) AND 'nurture' (our genetic engineering efforts with ALE) working in tandem towards a common goal.

Materials and methods

Microbiological and molecular methods

Lysogenic broth containing 50 $mg{\cdot}L^{-1}$ ampicillin was used for plasmid construction in *E. coli* NEB5α. *M. acetivorans* and *M. barkeri* were cultured in a high-salt medium tailored to the specific requirements of the experiment [62]. Depending on the experimental conditions, substrates were added as follows: 60 mM methanol alone (HSMe); 60 mM methanol combined with 60 mM formate (MF); a mixture of 60 mM methanol, 60 mM formate, along with 5 mM each of acetate and pyruvate (MFAcP); 120 mM formate alone (HSF); or a mixture of 120 mM formate, along with 5 mM each of acetate and pyruvate (HSFAcP). Media was supplemented with 1 $g{\cdot}L^{-1}$ casamino acids where specified. *M. maripaludis* was cultured in McFC medium as described previously [63]. Cultures were grown at 37 °C with the gas phase consisting of 50% N_2/20% CO_2/30% of 1% H_2S in N_2 at atmospheric pressure. The attenuance of the cultures was tracked using Eppendorf BioPhotometer plus spectrophotometer. DPI (Sigma-Aldrich, St Louis, MO, USA) was dissolved in dimethyl sulfoxide and added where mentioned to the media at a final concentration of 20 µM. Plasmid construction was carried out according to standard protocols. Liposome-mediated methods and polyethylene glycol-mediated methods were used to transform *M. acetivorans* [64]. An optimized CRISPR/Cas9 genome editing toolbox was used to delete genes [65,66]. The media composition, strains, primers and gRNA, as well as the plasmids used in the present study are listed in Tables S2, S3, S4 and S5, respectively.

Strain construction

The construction of strain JB-MF was achieved by introducing the recombinant fragment 'mtr::fdh P1P10' into *M. acetivorans* WWM73, followed by screening on MFAcP plates supplemented with 1 $g{\cdot}L^{-1}$ casamino acids and 2 $\mu g{\cdot}mL^{-1}$ puromycin. The 'mtr::fdh P1P10' fragment was generated through overlap PCR by concatenating fragments 'mtr::fdh P1P2', 'mtr::fdh P3P4', 'mtr::fdh P5P6', 'mtr::fdh P7P8' and 'mtr::fdh P9P10'. Fragments 'mtr::fdh P1P2' and 'mtr::fdh P9P10' were amplified using the *M. acetivorans* WWM73 genome as a template, whereas 'mtr::fdh P3P4' and 'mtr::fdh P5P6' utilized the *M. barkeri* WWM155 genome. The 'mtr::fdh P7P8' fragment was amplified from pM001. The excision of the *pac-hpt* selection marker from the strain was achieved by introducing the 'mtr::fdh P11P14' fragment into the previously mentioned strain. This fragment includes approximately 1.1 kb of homologous recombination regions upstream and downstream of the *pac-hpt* cassette. Following this introduction, counterselection was performed on MFAcP plates containing 20 $\mu g{\cdot}mL^{-1}$ 8-aza-2,6-diaminopurine. Strain

M. acetivorans JB-F1 was engineered by transforming PvuI-linearized pfdh V3 into *M. acetivorans* WWM73, followed by screening on HSMe plates with 2 $\mu g \cdot mL^{-1}$ puromycin. The pfdh V3 plasmid was assembled using Gibson assembly, incorporating fragments 'frh::fdh P15P16', 'frh::fdh P17P18', 'frh::fdh P19P20', 'frh::fdh P21P22', 'frh::fdh P23P24', 'frh::fdh P25P26', 'frh::fdh P27P28', and the *Apa*I and *Sac*I-digested p425GPD vector. The *pac-hpt* marker was excised through counterselection on HSMe plates containing 20 $\mu g \cdot mL^{-1}$ 8-aza-2,6-diaminopurine. The rest of the strains were constructed by transforming the corresponding plasmids. The assembly of additional plasmids was performed using Gibson cloning and Golden Gate cloning techniques, adhering to standard plasmid construction protocols [67,68].

Quantification of formate dehydrogenase activity

Here, 10 mL cultures of *M. acetivorans*, propagated on methanol, were harvested by centrifugation (5400 ***g***) for 10 min. Cleared cell-free lysates were prepared by resuspending the pellets in 1 mL potassium phosphate buffer (KP) (50 mM, pH 7.2) and incubating for 30 min on ice before centrifuging (5400 ***g*** for 10 min) again. Fdh activity was determined anaerobically in stoppered cuvettes (flushed with N_2) from the supernatant by following formate-dependent benzylviologen (BV) reduction (at 578 nm for 5 min); 1-mL assays consisted of 750 µL of KP, 100 µL of 1 M formate and 100 µL of BV (10 mM in KP); before starting the assay with 50 µL cleared cell-free lysate, BV was slightly pre-reduced with 10 µL of 100 mM Na-dithionite (until light blue); stock solutions were made anaerobic by repeated gas/vacuum cycles in stoppered vials; formate-independent BV reduction of the extract was subtracted from the values to account for unspecific oxidoreductase activity. Specific Fdh activity was calculated using an absorption coefficient for BV of 8.65 $mM^{-1} \cdot cm^{-1}$ [69] and is given in U (1 µmol BV reduced min^{-1}) mg^{-1} protein. All protein quantification was performed using the BCA Protein Assay Kit (Pierce, Waltham, MA, USA) and employing the method of Bradford [70].

Metabolite analyses

Methanol, formate and acetate were quantified using ^{1}H-NMR spectroscopy. Growth medium samples were complemented with 10% D_2O and 0.10% 1,4-dioxane as an internal standard for quantification. The ^{1}H-NMR spectroscopy measurements were performed at 298 K on a 400 MHz Bruker Avance III spectrometer (Bruker, Bremen, Germany) equipped with a 5-mm room temperature BBFO probe. Data acquisition was performed using TOPSPIN, version 3.6.2 (Bruker). The spectra were measured with a repetition time of 9.1 s over 16 scans using a 1D NOESY method with presaturation during relaxation delay and mixing time. The chemical shifts were calibrated on the signal of dioxane, set to 3.70 ppm. The integration values of peaks at 8.39 ppm for formate (s), 3.30 ppm for methanol (s) and 1.57 ppm for acetate (s) used for quantification. The methane level in the headspace gas sample was measured using gas chromatography-flame ionization detection (Agilent HP 6890 Gas Chromatograph; Agilent Technologies Inc., Santa Clara, CA, USA), equipped with an HP-Al/KCl column (length 50 m; diameter 0.32 mm, thickness 8 µm). The headspace gas samples were injected with a Gastight 1700 SampleLock Syringe (100 µL, PN81056) (Hamilton). The gas chromatography-flame ionization detection setup comprised the temperature of the front inlet set to 200 °C, that of the column oven to 40 °C (isothermal) and that of front detector to 250 °C. The pressure of the front inlet was set to 1.45 bar, and the total flow of helium was set to 15.2 $mL \cdot min^{-1}$. The mobile phase was hydrogen and synthetic air at a flow rate of 35 and 350 $mL \cdot min^{-1}$. The makeup flow was 26 $mL \cdot min^{-1}$ for helium.

ALE

M. acetivorans JB-F1 was initially cultivated in HSMe medium supplemented with 125 mM methanol (Transfer 1, T1). Subsequently, cells were washed twice using HS medium and then transferred (T2) to 10 mL of HSFAcP medium, supplemented with 1 $g \cdot L^{-1}$ casamino acids. After 4 weeks, 1 mL from T2 culture was transferred (T3) to another 10 mL of HSFAcP medium, supplemented with 1 $g \cdot L^{-1}$ casamino acids. After 23 days, 1 mL from the T3 culture was transferred (T4) to 10 mL of HSFAcP medium, containing 120 mM formate, 5 mM each of acetate and pyruvate. After 16 days, 1 mL from the T4 culture was transferred (T5) to 10 mL of HSF medium. Gas chromatography measurements were conducted from the T5 culture onward, ranging from every 4 days to daily, depending on the rate of methanogenesis. Once the exponential phase of methanogenesis finished, 1 mL of the culture was transferred to a fresh 10 mL of HSF medium. From T24 forward, the volume of inoculum was reduced to 200 µL to accommodate the increased growth rate.

Estimation of the free energy available after growth of strain JB-F2 on formate

Free energy for formate-dependent CO_2-reducing methanogenesis at standard conditions:

$$4\ HCOO^- + 4\ H^+ = 3\ CO_2 + CH_4 + 2\ H_2O$$

$\Delta G^\circ = -304.0\ kJ \cdot mol^{-1}$, $\Delta G^{\circ\prime} = -144.4\ kJ \cdot mol^{-1}$

The free energy (ΔG) is calculated according to: $\Delta G = \Delta G^\circ + RT\ \ln(K)$.

For simplicity, we provide the calculation of the thermodynamics at $T = 298$ K (25 °C, standard conditions), even

Table 5. Concentrations of products and residual substrates after incubation of JB-F2 with formate.

Species	Concentration	Comment
Formate ($HCOO^-$)	0.0115 M	Measured via ^{1}H-NMR spectroscopy
Protons (H^+)	1.58×10^{-8} M	Measured pH = 7.8
Methane (CH_4)	0.2 bar	Measured via gas chromatography
Carbon dioxide (CO_2)	0.2–1.2 bar	Estimation

though the incubations were at 37 °C. This estimation gives a value (error) that is approximately 1.5 kJ·mol^{-1} lower than if calculated at 310 K (37 °C, the actual incubation temperature).

K is defined as: $K = [CO_2]^3 \times [CH_4]/([HCOO^-]^4 \times [H^+]^4)$.

Concentrations of products and residual substrates after incubation of JB-F2 with formate can be found in Table 5.

The CO_2 partial pressure could not be directly measured. If all CO_2 derived from the consumed formate would end up in the headspace, a partial pressure of 1.2 bar would be obtained, which serves as the upper limit. When comparing methanogenesis by JB-F2 on formate vs. on methanol, we observed that growth on methanol leads to a much stronger pressure build-up compared to formate-dependent CO_2-reducing methanogenesis, even though, in both cases, the same amount of gas would be expected. The CO_2 formed from formate is putatively absorbed partly in the medium as a result of the pH increase. We therefore estimate 0.2 bar CO_2 as the lower limit, which corresponds to the initial partial pressure if all newly formed CO_2 would stay in solution.

Results of the thermodynamic calculations:

For a CO_2 partial pressure of 0.2 bar: $K = 1.45*10^{36}$, $\Delta G = -97.7$ kJ·mol^{-1}.

For a CO_2 partial pressure of 1.2 bar: $K = 3.13*10^{38}$, $\Delta G = -84.4$ kJ·mol^{-1}.

Taking uncertainties of other values into account (e.g. pH measurement, influence of temperature), we conclude that the free energy is between −100 and −80 kJ·mol^{-1}.

Assuming the calculated range of free energy and the ΔG for ATP formation is in the range 60–80 kJ·mol^{-1} [71], we can get an ATP yield of 1–1.67 ATP mol^{-1} CH_4.

Nucleic acid isolation, sequencing and analysis

The genomic DNA was extracted with Wizard Genomic DNA Purification Kit (Promega, Madison, WI, USA). The Microbial WGS was performed using Illumina NovaSeq 6000 by Novogene (UK) Company (Cambridge, UK). The resultant data was filtered using TRIMMOMATIC [72], aligned using BWA-MEM2 [73] to *M. acetivorans* C2A genome [55] (accession no AE010299) and analyzed for single nucleotide polymorphisms and SVs using SAMTOOLS [74] and BREAKDANCER [75]. For transcriptomics, the cultures were grown in triplicates to an OD_{600} of 0.3–0.4 and pelleted in RNAprotect (Qiagen, Hilden, Germany). RNA was isolated using a RNA isolation kit (Qiagen). The total RNA was sent to Novogene for library prep and sequencing. The resultant data were filtered using trimmomatic and analyzed using Geneious Prime 2023.1.2 Workbench (https://www.geneious.com). For genome reference for transcriptomics, *M. acetivorans* C2A genome (accession no AE010299) was modified to have four extra sequences reflecting CDS of fdhAB, tetR and phi31. The differential gene expression analysis was done using DESEQ2 [76] in Geneious Prime 2023.1.2 (https://www.geneious.com).

Database for phylogenetic analysis

The database used to search for FdhA homologs contains 10 864 prokaryote proteomes from NCBI and has been assembled in a previous study [5]. Several sampling steps were applied to assemble this database. First, we removed the redundancy based on taxonomic IDs. Second, we performed a whole genome comparison and used a clustering approach to group closest genomes, and then selected one representative genome per group. Third, we clustered the genomes by phylum/major clade and performed a clustering based on RpoB sequences. The representative genomes were selected using the NCBI completeness status, the NCBI representative status, the availability of annotation files and the number of proteins reviewed in Uniprot.

Phylogenetic analysis

We searched the homologs of FdhA using HMMsearch from HMMER v3.3.2 suite [77], using an HMM profile built from an alignment of several FdhA sequences. The sequences presenting a *e*-value < 0.01 were selected and aligned using MAFFT v7.490 [78] (default parameters). The alignment was trimmed using BMGE v1.12 [79] (-b 1 -w 1 -h 0.95 -m BLOSUM30 options) and the trimmed alignment has been used to infer a phylogenetic tree using FASTTREE v2.1.10 [80] (LG + G4). We then delineated the FdhA subfamily among the big homolog family using the topology, branch length and sequence length.

For the phylogenetic analysis, the sequences have been sampled using a selection of 401 bacteria [5] and 525 archaea (457 archaea corresponding to 1–15 genomes per major clade and 68 genomes of Methanosarcinales). We also added sequence of *M. mazei* identified by a BLASTp on NCBI, two sequences of other Methanosarcinales and two sequences of *Methanoflorentaceae* that were not present in the initial database. The sequences have been realigned using MAFFT-LINSI [78], and the resulting alignment has been manually curated. The alignment was then trimmed using

BMGE [79] (-b 1 -w 1 -h 0.95 -m BLOSUM30 options) and the trimmed alignment has been used to infer a phylogenetic tree using IQ-TREE v1.6.12 [81], using the best suited model according to the BIC (LG + R10). The robustness of the branches has been assessed by 1000 ultrafast bootstrap replicates. The figure was generated using ITOL [82].

Acknowledgements

We thank Professor Alfred Spormann, Dr Boyang Ji and Dr Christian Molina for helpful discussions. This research has received financial support from the Novo-Nordisk foundation (Grant no NNF19OC0054329 to SS and grant no NNF20OC0065032 to JB), the Research Council of Finland (Grant no 329510 to SS), Agence Nationale de la Recherche (Grant no ANR-19-CE02-0005-01 to GB), and the Bundesministerium für Bildung und Forschung (grant no 031B0851A to MR). We thank Professor William Metcalf (University of Illinois, USA), Professor Kyle Costa (University of Minnesota, USA) and Professor Nicole Buan (University of Nebraska-Lincoln, USA) for providing the strains and plasmids used in this study. We also acknowledge the Aalto University Raw Materials Research Infrastructures and Bioeconomy facilities.

Conflicts of interest

The authors declare that they have no conflicts of interest.

Author contributions

JB, TS and SS conceptualized the study. JB, TS, YT, MGL and CS performed the experiments. TS and JB analyzed the data. PSG and GB performed the phylogenetic analysis. SS, MR and GB supervised the experiments. TS, JB, GB and SS wrote the manuscript. All authors read and approved the final version of the manuscript submitted for publication.

Peer review

The peer review history for this article is available at https://www.webofscience.com/api/gateway/wos/peer-review/10.1111/febs.17409.

Data availability statement

All raw reads for whole-genome sequencing and transcriptomics have been uploaded to Sequence Read Archive database under the Bioproject PRJNA1085037 (https://www.ncbi.nlm.nih.gov/bioproject/?term=PRJNA1085037). All other study data are available in the published article and/or the Supporting information, as well as DRYAD (https://doi.org/10.5061/dryad.931zcrjvd).

References

1 Thauer RK, Kaster AK, Seedorf H, Buckel W & Hedderich R (2008) Methanogenic archaea: ecologically relevant differences in energy conservation. *Nat Rev Microbiol* **6**, 579–591.
2 Buan NR (2018) Methanogens: pushing the boundaries of biology. *Emerg Top Life Sci* **2**, 629–646.
3 Berghuis BA, Yu FB, Schulz F, Blainey PC, Woyke T & Quake SR (2019) Hydrogenotrophic methanogenesis in archaeal phylum Verstraetearchaeota reveals the shared ancestry of all methanogens. *Proc Natl Acad Sci U S A* **116**, 5037–5044.
4 Shima S, Huang G, Wagner T & Ermler U (2020) Structural basis of Hydrogenotrophic Methanogenesis. *Annu Rev Microbiol* **74**, 713–733.
5 Garcia PS, Gribaldo S & Borrel G (2022) Diversity and evolution of methane-related pathways in archaea. *Annu Rev Microbiol* **76**, 727–755.
6 Adam PS, Borrel G & Gribaldo S (2019) An archaeal origin of the Wood–Ljungdahl H4MPT branch and the emergence of bacterial methylotrophy. *Nat Microbiol* **4**, 2155–2163.
7 Mand TD & Metcalf WW (2019) Energy conservation and hydrogenase function in methanogenic archaea, in particular the genus Methanosarcina. *Microbiol Mol Biol Rev* **83**, e00020-19.
8 Thauer RK, Kaster AK, Goenrich M, Schick M, Hiromoto T & Shima S (2010) Hydrogenases from methanogenic archaea, nickel, a novel cofactor, and H2 storage. *Annu Rev Biochem* **79**, 507–536.
9 Kaster AK, Moll J, Parey K & Thauer RK (2011) Coupling of ferredoxin and heterodisulfide reduction via electron bifurcation in hydrogenotrophic methanogenic archaea. *Proc Natl Acad Sci U S A* **108**, 2981–2986.
10 Bertram PA & Thauer RK (1994) Thermodynamics of the Formylmethanofuran dehydrogenase reaction in *Methanobacterium thermoautotrophicum*. *Eur J Biochem* **226**, 811–818.
11 Laird MG, Adlung N, Koivisto JJ & Scheller S (2024) Thiol-disulfide exchange kinetics and redox potential of the coenzyme M and coenzyme B Heterodisulfide, an electron acceptor coupled to energy conservation in methanogenic archaea. *Chembiochem* **25**, e202300595.
12 Wagner T, Koch J, Ermler U & Shima S (2017) Methanogenic heterodisulfide reductase (HdrABC-MvhAGD) uses two noncubane [4Fe-4S] clusters for reduction. *Science* **357**, 699–703.

13 Lyu Z, Shao N, Akinyemi T & Whitman WB (2018) Methanogenesis. *Curr Biol* **28**, R727–R732.
14 Baron SF & Ferry JG (1989) Reconstitution and properties of a coenzyme F420-mediated formate hydrogenlyase system in *Methanobacterium formicicum*. *J Bacteriol* **171**, 3854–3859.
15 Costa KC, Wong PM, Wang T, Lie TJ, Dodsworth JA, Swanson I, Burn JA, Hackett M & Leigh JA (2010) Protein complexing in a methanogen suggests electron bifurcation and electron delivery from formate to heterodisulfide reductase. *Proc Natl Acad Sci U S A* **107**, 11050–11055.
16 Meuer J, Kuettner HC, Zhang JK, Hedderich R & Metcalf WW (2002) Genetic analysis of the archaeon *Methanosarcina barkeri* fusaro reveals a central role for ech hydrogenase and ferredoxin in methanogenesis and carbon fixation. *Proc Natl Acad Sci U S A* **99**, 5632–5637.
17 Blaut M (1994) Metabolism of methanogens. *Antonie Van Leeuwenhoek* **66**, 187–208.
18 Lie TJ, Costa KC, Lupa B, Korpole S, Whitman WB & Leigh JA (2012) Essential anaplerotic role for the energy-converting hydrogenase Eha in hydrogenotrophic methanogenesis. *Proc Natl Acad Sci U S A* **109**, 15473–15478.
19 Porat I, Kim W, Hendrickson EL, Xia Q, Zhang Y, Wang T, Taub F, Moore BC, Anderson IJ, Hackett M *et al.* (2006) Disruption of the operon encoding Ehb hydrogenase limits anabolic CO_2 assimilation in the archaeon *Methanococcus maripaludis*. *J Bacteriol* **188**, 1373–1380.
20 Lyu Z & Liu Y (2019) Diversity and taxonomy of methanogens. In Biogenesis of Hydrocarbons. Handbook of Hydrocarbon and Lipid Microbiology (Stams A & Sousa D, eds), pp. 19–77. Springer, Cham.
21 Fu H & Metcalf WW (2015) Genetic basis for metabolism of methylated sulfur compounds in *Methanosarcina* species. *J Bacteriol* **197**, 1515–1524.
22 Rother M & Metcalf WW (2004) Anaerobic growth of *Methanosarcina acetivorans* C2A on carbon monoxide: an unusual way of life for a methanogenic archaeon. *Proc Natl Acad Sci U S A* **101**, 16929–16934.
23 Welte C & Deppenmeier U (2014) Bioenergetics and anaerobic respiratory chains of aceticlastic methanogens. *Biochim Biophys Acta Bioenerg* **1837**, 1130–1147.
24 Buan NR & Metcalf WW (2010) Methanogenesis by *Methanosarcina acetivorans* involves two structurally and functionally distinct classes of heterodisulfide reductase. *Mol Microbiol* **75**, 843–853.
25 Yan Z, Wang M & Ferry JG (2017) A ferredoxin- and F420H2-dependent, electron-bifurcating, Heterodisulfide reductase with homologs in the domains bacteria and archaea. *MBio* **8**, e02285-16.
26 Guss AM, Kulkarni G & Metcalf WW (2009) Differences in hydrogenase gene expression between *Methanosarcina acetivorans* and *Methanosarcina barkeri*. *J Bacteriol* **191**, 2826–2833.
27 Guss AM, Mukhopadhyay B, Zhang JK & Metcalf WW (2005) Genetic analysis of mch mutants in two Methanosarcina species demonstrates multiple roles for the methanopterin-dependent C-1 oxidation/reduction pathway and differences in H2 metabolism between closely related species. *Mol Microbiol* **55**, 1671–1680.
28 Mand TD, Kulkarni G & Metcalf WW (2018) Genetic, biochemical, and molecular characterization of *Methanosarcina barkeri* mutants lacking three distinct classes of hydrogenase. *J Bacteriol* **200**, e00342-18.
29 Kuhns M, Trifunović D, Huber H & Müller V (2020) The Rnf complex is a Na+ coupled respiratory enzyme in a fermenting bacterium, *Thermotoga maritima*. *Commun Biol* **3**, 431.
30 Hess V, Schuchmann K & Müller V (2013) The ferredoxin: NAD+ oxidoreductase (Rnf) from the acetogen *Acetobacterium woodii* requires na+ and is reversibly coupled to the membrane potential. *J Biol Chem* **288**, 31496–31502.
31 Mazumder TK, Nishio N & Nagai S (1985) Carbon monoxide conversion to formate by *Methanosarcina barkeri*. *Biotechnol Lett* **7**, 377–382.
32 Maeder DL, Anderson I, Brettin TS, Bruce DC, Gilna P, Han CS, Lapidus A, Metcalf WW, Saunders E, Tapia R *et al.* (2006) The *Methanosarcina barkeri* genome: comparative analysis with *Methanosarcina acetivorans* and *Methanosarcina mazei* reveals extensive rearrangement within methanosarcinal genomes. *J Bacteriol* **188**, 7922–7931.
33 Youngblut ND, Wirth JS, Henriksen JR, Smith M, Simon H, Metcalf WW & Whitaker RJ (2015) Genomic and phenotypic differentiation among *Methanosarcina mazei* populations from Columbia River sediment. *ISME J* **9**, 2191–2205.
34 Holden JF & Sistu H (2023) Formate and hydrogen in hydrothermal vents and their use by extremely thermophilic methanogens and heterotrophs. *Front Microbiol* **14**, 1093018.
35 Kammel M & Gary Sawers R (2022) The FocA channel functions to maintain intracellular formate homeostasis during *Escherichia coli* fermentation. *Microbiology* **168**, 001168.
36 Ribas D, Soares-Silva I, Vieira D, Sousa-Silva M, Sá-Pessoa J, Azevedo-Silva J, Viegas SC, Arraiano CM, Diallinas G, Paiva S *et al.* (2019) The acetate uptake transporter family motif "NPAPLGL(M/S)" is essential for substrate uptake. *Fungal Genet Biol* **122**, 1–10.
37 Rendulić T, Alves J, Azevedo-Silva J, Soares-Silva I & Casal M (2021) New insights into the acetate uptake transporter (AceTr) family: unveiling amino acid

residues critical for specificity and activity. *Comput Struct Biotechnol J* **19**, 4412–4425.
38 Feldewert C, Lang K & Brune A (2021) The hydrogen threshold of obligately methyl-reducing methanogens. *FEMS Microbiol Lett* **367**, fnaa137.
39 Steiniger F, Sorokin DY & Deppenmeier U (2022) Process of energy conservation in the extremely haloalkaliphilic methyl-reducing methanogen *Methanonatronarchaeum thermophilum*. *FEBS J* **289**, 549–563.
40 Sorokin DY, Makarova KS, Abbas B, Ferrer M, Golyshin PN, Galinski EA, Ciordia S, Mena MC, Merkel AY, Wolf YI *et al.* (2017) Discovery of extremely halophilic, methyl-reducing euryarchaea provides insights into the evolutionary origin of methanogenesis. *Nat Microbiol* **2**, 17081.
41 Borrel G, Adam PS, McKay LJ, Chen LX, Sierra-García IN, Sieber CMK, Letourneur Q, Ghozlane A, Andersen GL, Li WJ *et al.* (2019) Wide diversity of methane and short-chain alkane metabolisms in uncultured archaea. *Nat Microbiol* **4**, 603–613.
42 Guss AM, Rother M, Zhang JK, Kulkarni G & Metcalf WW (2008) New methods for tightly regulated gene expression and highly efficient chromosomal integration of cloned genes for Methanosarcina species. *Archaea* **2**, 193–203.
43 Schöne C, Poehlein A, Jehmlich N, Adlung N, Daniel R, von Bergen M, Scheller S & Rother M (2022) Deconstructing *Methanosarcina acetivorans* into an acetogenic archaeon. *Proc Natl Acad Sci U S A* **119**, e2113853119.
44 Schöne C, Poehlein A & Rother M (2023) Genetic and physiological probing of cytoplasmic bypasses for the energy-converting Methyltransferase Mtr in *Methanosarcina acetivorans*. *Appl Environ Microbiol* **89**, e02161-22.
45 Ferry JG (2020) *Methanosarcina acetivorans*: a model for mechanistic understanding of Aceticlastic and reverse Methanogenesis. *Front Microbiol* **11**, 1806.
46 Suharti S, Wang M, De Vries S & Ferry JG (2014) Characterization of the RnfB and RnfG subunits of the Rnf complex from the archaeon *Methanosarcina acetivorans*. *PLoS One* **9**, e97966.
47 Matschiavelli N & Rother M (2015) Role of a putative tungsten-dependent formylmethanofuran dehydrogenase in *Methanosarcina acetivorans*. *Arch Microbiol* **197**, 379–388.
48 Brodersen J, Bäumer S, Abken HJ, Gottschalk G & Deppenmeier U (1999) Inhibition of membrane-bound electron transport of the methanogenic archaeon *Methanosarcina mazei* Go1 by diphenyleneiodonium. *Eur J Biochem* **259**, 218–224.
49 Huser BA, Wuhrmann K & Zehnder AJB (1982) *Methanothrix soehngenii* gen. Nov. sp. nov., a new acetotrophic non-hydrogen-oxidizing methane bacterium. *Arch Microbiol* **132**, 1–9.
50 Kamagata Y & Mikami E (1991) Isolation and characterization of a novel thermophilic *Methanosaeta* strain. *Int J Syst Bacteriol* **41**, 191–196.
51 Ma K, Liu X & Dong X (2006) *Methanosaeta harundinacea* sp. nov., a novel acetate-scavenging methanogen isolated from a UASB reactor. *Int J Syst Evol Microbiol* **56**, 127–131.
52 Wagner D (2020) Methanosarcina. In Bergey's Manual of Systematics of Archaea and Bacteria (Trujillo ME, Dedysh S, DeVos P, Hedlund B, Kämpfer P, Rainey FA & Whitman WB, eds), pp. 1–23. John Wiley & Sons, Ltd, Hoboken, NJ.
53 Zhou J, Smith JA, Li M & Holmes DE (2023) Methane production by Methanothrix thermoacetophila via direct interspecies electron transfer with *Geobacter metallireducens*. *MBio* **14**, e00360-23.
54 Thomé R, Gust A, Toci R, Mendel R, Bittner F, Magalon A & Walburger A (2012) A sulfurtransferase is essential for activity of formate dehydrogenases in *Escherichia coli*. *J Biol Chem* **287**, 4671–4678.
55 Galagan JE, Nusbaum C, Roy A, Endrizzi MG, Macdonald P, Fitzhugh W, Calvo S, Engels R, Smirnov S, Atnoor D *et al.* (2002) The genome of *M. acetivorans* reveals extensive metabolic and physiological diversity. *Genome Res* **12**, 532–542.
56 Buckel W & Thauer RK (2018) Flavin-based electron bifurcation, ferredoxin, flavodoxin, and anaerobic respiration with protons (Ech) or NAD+ (Rnf) as electron acceptors: a historical review. *Front Microbiol* **9**, 401.
57 Poudel S, Dunham EC, Lindsay MR, Amenabar MJ, Fones EM, Colman DR & Boyd ES (2018) Origin and evolution of flavin-based electron bifurcating enzymes. *Front Microbiol* **9**, 1762.
58 Holmes DE, Rotaru AE, Ueki T, Shrestha PM, Ferry JG & Lovley DR (2018) Electron and proton flux for carbon dioxide reduction in *Methanosarcina barkeri* during direct interspecies electron transfer. *Front Microbiol* **9**, 3109.
59 Halim MFA, Day LA & Costa KC (2021) Formate-dependent Heterodisulfide reduction in a *Methanomicrobiales archaeon*. *Appl Environ Microbiol* **87**, e02698-20.
60 Costa KC, Lie TJ, Xia Q & Leigh JA (2013) VhuD facilitates electron flow from H2 or formate to heterodisulfide reductase in *Methanococcus maripaludis*. *J Bacteriol* **195**, 5160–5165.
61 Gupta D, Chen K, Elliott SJ & Nayak DD (2024) MmcA is an electron conduit that facilitates both intracellular and extracellular electron transport in *Methanosarcina acetivorans*. *Nat Commun* **15**, 3300.
62 Sowers KR, Boone JE & Gunsalus RP (1993) Disaggregation of Methanosarcina spp. and growth as single cells at elevated Osmolarity. *Appl Environ Microbiol* **59**, 3832–3839.

63 Bao J, De Dios Mateos E & Scheller S (2022) Efficient CRISPR/Cas12a-based genome-editing toolbox for metabolic engineering in *Methanococcus maripaludis*. *ACS Synth Biol* **11**, 2496–2503.
64 Metcalf WW, Zhang JK, Apolinario E, Sowers KR & Wolfe RS (1997) A genetic system for archaea of the genus *Methanosarcina*: liposome-mediated transformation and construction of shuttle vectors. *Proc Natl Acad Sci U S A* **94**, 2626–2631.
65 Zhu P, Somvanshi T, Bao J & Scheller S (2023) CRISPR/Cas12a toolbox for genome editing in *Methanosarcina acetivorans*. *Front Microbiol* **14**, 1235616.
66 Nayak DD & Metcalf WW (2017) Cas9-mediated genome editing in the methanogenic archaeon *Methanosarcina acetivorans*. *Proc Natl Acad Sci U S A* **114**, 2976–2981.
67 Gibson DG, Young L, Chuang RY, Venter JC, Hutchison CA & Smith HO (2009) Enzymatic assembly of DNA molecules up to several hundred kilobases. *Nat Methods* **6**, 343–345.
68 Engler C, Kandzia R & Marillonnet S (2008) A one pot, one step, precision cloning method with high throughput capability. *PLoS One* **3**, e3647.
69 Hedderich R, Berkessel A & Thauer RK (1989) Catalytic properties of the heterodisulfide reductase involved in the final step of methanogenesis. *FEBS Lett* **255**, 67–71.
70 Bradford MM (1976) A rapid and sensitive method for the quantitation of microgram quantities of protein utilizing the principle of protein-dye binding. *Anal Biochem* **72**, 248–254.
71 Buckel W & Thauer RK (2013) Energy conservation via electron bifurcating ferredoxin reduction and proton/Na+ translocating ferredoxin oxidation. *Biochim Biophys Acta Bioenerg* **1827**, 94–113.
72 Bolger AM, Lohse M & Usadel B (2014) Trimmomatic: A flexible trimmer for Illumina sequence data. *Bioinformatics* **30**, 2114–2120.
73 Md V, Misra S, Li H & Aluru S (2019) Efficient architecture-aware acceleration of BWA-MEM for multicore systems. In Proceedings – 2019 IEEE 33rd International Parallel and Distributed Processing Symposium, IPDPS 2019, 314–324.
74 Li H, Handsaker B, Wysoker A, Fennell T, Ruan J, Homer N, Marth G, Abecasis G & Durbin R (2009) The sequence alignment/map format and SAMtools. *Bioinformatics* **25**, 2078–2079.
75 Chen K, Wallis JW, McLellan MD, Larson DE, Kalicki JM, Pohl CS, McGrath SD, Wendl MC, Zhang Q, Locke DP *et al.* (2009) BreakDancer: an algorithm for high-resolution mapping of genomic structural variation. *Nat Methods* **6**, 677–681.
76 Love MI, Huber W & Anders S (2014) Moderated estimation of fold change and dispersion for RNA-seq data with DESeq2. *Genome Biol* **15**, 1–21.
77 Eddy SR (2011) Accelerated profile HMM searches. *PLoS Comput Biol* **7**, e1002195.
78 Katoh K & Standley DM (2013) MAFFT multiple sequence alignment software version 7: improvements in performance and usability. *Mol Biol Evol* **30**, 772–780.
79 Criscuolo A & Gribaldo S (2010) BMGE (block mapping and gathering with entropy): a new software for selection of phylogenetic informative regions from multiple sequence alignments. *BMC Evol Biol* **10**, 210.
80 Price MN, Dehal PS & Arkin AP (2010) FastTree 2 – approximately maximum-likelihood trees for large alignments. *PLoS One* **5**, e9490.
81 Nguyen LT, Schmidt HA, Von Haeseler A & Minh BQ (2015) IQ-TREE: a fast and effective stochastic algorithm for estimating maximum-likelihood phylogenies. *Mol Biol Evol* **32**, 268–274.
82 Letunic I & Bork P (2021) Interactive tree of life (iTOL) v5: an online tool for phylogenetic tree display and annotation. *Nucleic Acids Res* **49**, W293–W296.
83 Schöne C & Rother M (2019) Methanogenesis from carbon monoxide. In Biogenesis of Hydrocarbons. Handbook of Hydrocarbon and Lipid Microbiology (Stams A & Sousa D, eds), pp. 123–151. Springer, Cham.

Supporting information

Additional supporting information may be found online in the Supporting Information section at the end of the article.

Dataset S1. Differential gene expression analysis of *M. acetivorans* WWM73 growing on HSMe compared to MF.

Dataset S2. Differential gene expression analysis of *M. acetivorans* JBA01 growing on MFAcP compared to MF.

Dataset S3. Differential gene expression analysis of *M. acetivorans* JBAF02 growing on HSMe compared to HSF.

Table S1. Single nucleotide polymorphisms found in ALE.

Table S2. Media composition.

Table S3. Strains used in the present study.

Table S4. Primers and gRNA used in the present study.

Table S5. Plasmids used in the present study.